DESIS

ATBD L1A, L1B, L1C, L2A Processors

Doc. ID	PAV-DLR-TN-004
Issue	1.3
Date	2015-07-20

DLR

SIGNATURES

Prepared	Janja Avbelj	
	Name/Organization	
Reviewed	Emiliano Carmona	
	Name/Organization	
Approved	Rupert Müller	
	Name/Organization	

DOCUMENT PREPARATION

The document on hand was prepared with contributions from personnel as listed below.

Janja, Avbelj	MF-PBA
(First Name, Last Name)	
Harald, Krawczyk	MF-PBA
(First Name, Last Name)	
Rupert, Müller	MF-PBA
(First Name, Last Name)	
Aliaksei, Makarau	MF-PBA
(First Name, Last Name)	
Martin, Bachmann	DFD-LAX
(First Name, Last Name)	
Valentin, Ziel	DFD-LAX
(First Name, Last Name)	
Raquel, de los Reyes	MF-PBA
(First Name, Last Name)	
Birgit, Gerasch	MF-PBA
(First Name, Last Name)	
Kevin, Alonso Gonzalez	MF-PBA
(First Name, Last Name)	
Emiliano, Carmona	MF-PBA
(First Name, Last Name)	

DISTRIBUTION LIST

Public

CHANGE RECORD

Issue	Date	Chapter	Change
1.0	20.07.2015	all	first issue
1.1	29.08.2015	Sections: 6.3.4, 7.4., 2.1	On reply to RID 31, RID 65, RID 66 and RID 67
1.1	08.09.2015	Section 6.4	On reply to RID 109 and RID 111
1,1	08.09.2015	Section 5.4	Added Auxiliary MUSES data as input data for L1A processor with TBD13 and TBD14 about the missing information on these data. Answer to CDR RID-100
1.1	09.09.2015	Section 5	Higher processing levels of stereo mode data takes are added and a TBD is formulated and referenced for currently unknown modes and parameters of the instrument. On reply to RID 96
1.1	09.09.2015	Section 7.4.4	Leverarm ISS-GPS to sensor projection center added to formula. On reply to RID 114.
1.1	15.09.2015	Sections 8.10 and A.1	Removed according to the RID 35.
1.1	15.09.2015	Section 8.4	Updated according to the RID 34.
1.1	15.09.2015	Section 8.10	Updated according to the RID 36.
1.1	15.09.2015	Figure 5-1, Section 5, and 5.6	Figure updated. Details on processing of the stereo mode added. On reply to RID 97. Comment and TBD was inserted in section 5.6 with regard to the screening and DC extraction processing of the Experimental Mode products.
1.1	15.09.2015	Figure 5-1, Section 5.5.4	Changed order of 1) Dead pixel mask and 2) Quality quicklook changed in Figure 5-1. Added explanation about not reprocessing of L1A data. On reply to RID 98.
1.1	15.09.2015	Section 5.2, 7.7.1	Time Synchronisation Concept document is added to the applicable documents table and referred to. The TBD about time synchronisation is removed. The name of the variable for time synchronisation is changed to t_FSync. On reply to RID 99.
1.1	15.09.2015	Section 5.4.2	Background value added. On reply to RID 104
1.1	15.09.2015	Section 5.1, Figure 5-1	Functionality of L1B processor is needed to create quicklooks. Figure 5-1 is updated. On reply to RID 105.
1.1	15.09.2015	Section 7.1	Rolling shutter is a baseline configuration. On reply to RID 112. The 13 cm shift between lines for DESIS is removed, because the read out of the chip is different.
1.1	15.09.2015	Figure 7-2	Figure updated. On reply to RID 113
1.1	17.09.2015	Sections:	On reply to RID 65, RID 66 and RID 67. Added two applicable docu-

Issue	Date	Chapter	Change
		7.4., 2.1	ments.
1.1	21.09.2015	Section 5.3.3	Description of dark value averaging changed in response to CDR RID 102
1.1	21.09.2015	Section 5.4.1	Justification for time interpolation of dark values added in response to CDR RID 103
1.1	23.09.2015	Section 6.3.3	Comment regarding FWHM added in response to RID 108
1.1	23.09.2015	Sections 6.2, 6.3	Order of NLC and DC changed in result of discussion with DLR-OS: first Dark correction, then non-linearity correction. (CDR RID 107)
1.1	02.10.2015	Sections 8.3 and 8.10	Mentioning that water, land and snow masks have to be visible in the image (CDR RID 135)
1.1	05.10.2015	Section 6.4 and 7.9 and 8.10	Updating quality layers definition following RIDs and subsequent discussions
1.1.	05.10.2015	Section 6.2	On reply to RID 106, the terminology for Reference table and Calibration data packages is harmonized with [AD04].
1.1	20.01.2017	Section 6.3	Corrected the explanation of the processing algorithm. Updated eq. 6-1 and eq. 6-3, now 6-5).
1.1	15.02.2017	Sections 6.4, 6.4.2, 8.10	Replaced band-to-band correlation matrix with detector map
1.1	10.04.2017	Section 6	Modified flowchart of **Fehler! Verweisquelle konnte nicht gefunden werden.**. In consequence new subsections are introduced: subsection 6.6 defines the interpolation method of the abnormal pixels, subsection 0 describes the rolling shutter correction (previously 7.1), subsection 0 defines the smile correction, and 6.8.2 the keystone correction.
1.1	08.05.2017	Section 7.3.2	Based on the geometric laboratory calibration procedure of the DESIS instrument the internal geometry has been updated
1.1	23.05.2017	Document preparation table	Responsibility for S-130 changed from Gregoire Kerr to Martin Bachmann and Valentin Ziel
1,1	02.06.2017	Section 5.4.2	Introduced the duplicated first row for better RS correction
1,1	19.07.2017	Section 6.3	Explained that the dark current subtraction is done with non-linearity corrected dark currents values.
1.1	01.08.2017	Fig. 3-1 Chapter 6.4	Corrected Fig. 3-1 Updated and extended Chapter 6.4
1.1	22.08.2017	Section 6 and 7	Updated figure and table names, updated list and table of contents

Issue	Date	Chapter	Change
1.1	06.09.2018	Section 5.3	Screening section was revised.
1.2	10.09.2018	Section 7.3.2.1	POI conversion updated
1.3	04.03.2019	5.3 7.7 7.8	Screening updated Sensor model improvement detailed QL resampling described
1.3	19.08.2019	6.3.3	Added more detail to the Radiometric Correction section

CONTENTS

1. Introduction 12
1.1 Purpose 12
1.2 Scope 12
2. References 13
2.1 Applicable Documents 13
2.2 Reference Documents 13
3. Terms and Abbreviations 17
3.1 Definition and indexing of an image cube 17
4. Processor Overview 20
5. Transcription Processor L1A 22
5.1 Overview 22
5.2 Raw Data and Virtual Channel 23
5.3 Screening 24
5.3.1 Temperatures 25
5.3.2 CRC 26
5.3.3 Dark current screening 26
5.3.4 Instrument Operational Parameters Metadata 27
5.4 Earth Data 27
5.4.1 Dark current extraction 28
5.4.2 Tiling of the DESIS data 29
5.4.3 Dead pixel mask 30
5.4.4 Quicklook generation 30
5.5 Calibration Measurement Data 30
5.6 Experimental Products 30
6. Systematic and Radiometric Correction Processor L1B 31
6.1 Overview 31
6.2 Input 31
6.3 Processing Algorithm 32
6.3.1 Non-Linearity Correction 33
6.3.2 Dark Signal Correction 33
6.3.3 Radiometric Correction 33
6.4 Quality Indicators Generation 34
6.4.1 Analysis for abnormal pixels 35
6.4.2 Calculation of the detector maps 35
6.4.3 Analysis for stripping and banding 36
6.4.4 Analysis for spectral smile indication 39
6.5 Spectral Referencing 41
6.6 Abnormal Pixel Interpolation 41
6.7 Rolling Shutter 42
6.8 Smile and Keystone Correction 44
6.8.1 Smile Correction 44
6.8.2 Keystone Correction 44
6.9 Radiometric Referencing 44
6.10 Output Specification 45
7. Geometric Correction Processor L1C 46
7.1 Input 46
7.2 DESIS/MUSES Coordinate Frames 47

7.3 Direct Georeferencing and Line-of-Sight Model 47
7.3.1 DESIS Interior Orientation 48
7.3.2 DESIS Instrument Mounting Angles (Boresight Alignment) 50
7.3.3 Atmospheric Refraction Correction 52
7.3.4 Exterior Orientation 53
7.3.5 Time Synchronisation and Interpolation 55
7.4 DEM Intersection Model 56
7.4.1 Global DEM Database 56
7.4.2 Iterative Determination of Object Points 58
7.5 Map Projection 60
7.6 Resampling 60
7.6.1 Nearest Neighbour 62
7.6.2 Bilinear 62
7.6.3 Cubic Convolution 62
7.7 Sensor Model Improvement 63
7.8 Quality Mask Generation 64
7.9 Output Specification 64

8. Atmospheric Correction Processor L2A 65
8.1 Input 65
8.2 Algorithm Description 65
8.3 Masks for land, water, haze, cloud, shadow 66
8.3.1 Water class 67
8.3.2 Cloud over land 67
8.3.3 Snow 68
8.3.4 Shadow 68
8.4 Radiative transfer calculations and atmospheric database 68
8.5 Extra-terrestrial solar irradiance spectrum 70
8.6 Retrieval of aerosol optical thickness 71
8.7 Retrieval of columnar water vapour 72
8.8 Retrieval of surface reflectance in flat terrain 73
8.9 Retrieval of surface reflectance in mountainous terrain 75
8.10 Input: Land Surface Temperature (LST) database 78
8.11 Output files 78
8.12 L2A quality flags 79

Appendix A 81
8.13 Appendix: Altitude profile of summer and winter atmospheres 81
A.1 Appendix: Selection of atmospheric LUTs 82
A.1.1 Appendix: LUT names 82

9. Open Issues 83

LIST OF FIGURES

Figure 3-1 HSI image cube and indexing 18
Figure 4-1 Processing Overview and Product Tree 21
Figure 5-1 Overview of the Transcription Processor L1A. Three different modes of raw DESIS Data are processed by the L1A Processor, these are: Earth Data Take, Calibration Data Take and Experimental Mode Data Take. The outputs of the L1A processor are L1A Earth Product, L1A Calibration Product, L1A Dark Current Product and L1A Experimental Mode Product, which are all archived in the corresponding long term archive. Additionally, metadata, virtual channel data and other axillary data are also stored as a part of the products. 23
Figure 5-2 Tiling of the DESIS Earth Data Take. First, the DC before and after each Earth DT is extracted. Then, the Spectral Images (SI) is tiled into $\boldsymbol{N}$ tiles with a size $(\mathbf{1024}+\mathbf{2}*\mathbf{8})\times\boldsymbol{Nj}\times\boldsymbol{Nk}$. There is an 8 lines overlap between subsequent tiles. Tiles delivered to the user are without overlap, and have a size of $\mathbf{1024}\times\mathbf{1024}$. 29
Figure 6-1 Overview of the Systematic and Radiometric Correction Processor L1B 32
Figure 6-2 Relationship between Abnormal pixels and calibration curve 35
Figure 6-3 Schematic concept of the detector map (example based on HySpex SWIR data). 36
Figure 6-4 Example using HySpex data for the detection of striping and the de-calibrated detector elements causing striping. On the left: normalized detector map of a single HySpex SWIR scene, incl. zoom on the detector element in question. Top-right: part of the HySpex image of band 31; bottom-right: cross-track radiance profile of band 31. 38
Figure 6-5 Example for analysing multiple HySpex detector maps. 39
Figure 6-6 Example for a radiance spectrum measured with ~ 3nm bandwidth from 350-1000nm and ~10nm for wavelength >1000nm; Fraunhofer lines in green, Water Vapor absorptions in blue, gas absorptions in red. Note that DN values are given for the radiance because of a known de-calibration of the measurements. 40
Figure 6-7 Illustration for the detection of uncorrected spectral smile using the Detector Maps of 82 airbrone HySpex datasets. Note that the SWIR wavelength region is depicted in this example, but the same principle is valid also for the VNIR wavelength region using different atmospheric absorption bands (see Fig. 6-6). 41
Figure 6-8 Rolling shutter and time delay of exposure of subsequent scan lines (rows) in one frame. 43
Figure 6-9 Influence of Smile and Keystone effects on the sensor geometry. 44
Figure 7-1 Overview of the Systematic and Radiometric Correction Processor L1B. 47
Figure 7-2 Direct Georeferencing (basic relation) 48
Figure 7-3 Schematic diagram of the POI 50
Figure 7-4 Global ASTER DEM [RD45]. 57
Figure 7-5 Method of determination of the actual sensor look direction with the DEM by an iterative approach. 58
Figure 7-6 Polygons (triangles) of the input image, defined by the centre of adjacent pixels, are transformed to the pixel grid of the orthoimage and filled with bilinear interpolated pixel value 61
Figure 8-1 Processing of land scenes. 65
Figure 8-2 Sequence of masking steps before starting the atmospheric correction. 68
Figure 8-3 Influence of ozone on surface reflectance retrieval. 69
Figure 8-4 Relative deviation (Kurucz2005 – Kurucz1997) / Kurucz1997 70
Figure 8-5 Schematic sketch of APDA method with three channels. 72
Figure 8-6 Treatment of the adjacency effect. 74
Figure 8-7 Radiation components in mountainous terrain. 75
Figure 8-8 SPOT-5 scene from Switzerland with topographic correction 78

LIST OF TABLES

Table 2-1 Applicable Documents 13
Table 2-2 Reference Documents 16
Table 3-1 Spaces and sub-spaces of an image cube. 19
Table 5-1 Parameters of Screening....24
Table 5-2 Parameters of Earth Data Processing....28
Table 6-1 Parameters for systematic and Radiometric Correction Processor L1B....31
Table 6-2 Summary of inputs and outputs in terms of quality indicators....34
Table 7-1 Parameters for Geometric Correction Processor L1C 46
Table 7-2 Design values of mirror mounting angles....50
Table 7-3 Relation between POI step and POI angle (preliminary settings)....51
Table 7-4 The magnitude of the ground displacement caused by atmospheric refraction as a function of off nadir view in space [RD44] 53
Table 7-5 GDEM characteristics [RD45]. 57
Table 7-6 Displacements caused by the DEM error for flat and mountainous area. 58
Table 7-7 Supported map projections (user input). 60
Table 7-8 Supported image resampling methods (user input). 61
Table 8-1 Parameters for Atmospheric Correction Processor L2A 65
Table 8-2 Enhanced classes (land, water, haze, cloud, etc.) 66
Table 8-3 Grid points in the atmospheric database. 70
Table 8-4 L2A quality flags....80
Table 9-1 List of TBD 84

1. Introduction

1.1 Purpose

The Algorithm Theoretical Basis Document (ATBD) shall help a reader to understand how DESIS L1A, L1B, L1C and L2A products are derived. The ATBD for L1A, L1B, L1C and L2A product generation describes algorithms for data transcription, systematic, radiometric, geometric and atmospheric processing of the raw DESIS hyperspectral data. The content of the document is as far as possible self-contained for external use. For the overview including mission, satellite and instrument characteristics see [AD06]. The text boxes in this document refer to the metadata described in [AD04].

1.2 Scope

Development of the algorithms for L1A, L1B, L1C and L2A product generation is a part of the Ground segment S-200 named DESIS Development Processor (DEV) [AD02] and is also valid for the TBE licensed SW.

2. References

2.1 Applicable Documents

The following documents contain provisions which, through reference in the document on hand, become applicable to the extent specified herein.

Applicability ID and Document Title	Document ID and Issue
[AD01] Products Specification	PAV-DLR-ICD-002 1.0
[AD02] Product Tree	PAV-DLR-TN-004 1.0
[AD03] File Format Interface Control Document	MUS DLR -IC-001, 1.0
[AD04] Data Product Specifications	PAV-DLR-ICD-002 1.0
[AD05] Ground Segment Requirements	PAV-DLR-RSP-001 1.1
[AD06] Ground Segment Overview	PAV-DLR-DD-001 1.0
[AD07] Glossary and Abbreviations	PAV-DLR-TN-005 1.0
[AD08] ATBD Vicarious Validation	PAV-DLR-TN-003 1.0
[AD09] DESIS Calibration Concept	PAV-DLR-TN-002 1.0
[AD10] Time Synchronisation Concept	MUS-DLR-TN-009 1.0
[AD11] Rolling Shutter Mode Operational Concept	MUS-DLR-TN-001 1.0
[AD12] DESIS Image File Screening Specification	MUS-DLR-RS-016 1.1

Table 2-1 Applicable Documents

2.2 Reference Documents

Standards listed below have been used (in the sense of tailoring) to prepare the document on hand. Documents which are recognized best practices are listed for the purpose of information.

Reference ID and Document Title	
[RD01]	Ground Systems and Operations – Part 1: Principles and requirements
[RD02]	Software – Part 1: Principles and requirements
[RD03]	System Engineering
[RD04]	Ackerman, S. A., Strabala, K. I., Menzel, W. P., Frey, R. A., Moeller, C. C., and Gumley, L. E., ”Discriminating clear sky from clouds with MODIS”, J. Geophys. Res., Vol. 103, D24, 32,141-32,157 (1998).
[RD05]	Berk, A., et al., “MODTRAN cloud and multiple scattering upgrades with application to AVIRIS”, Remote Sensing of Environment, Vol. 65, 367-375 (1998).
[RD06]	Berk, A., et al., “MODTRAN4 Version 3 Revision 1 User‘s Manual", Air Force Research Laboratory, Hanscom MA (2003).
[RD07]	Berk, A., Anderson, G.P., Acharya, P.K., and Shettle, E.P., “MODTRAN5.2.0.0 User’s Manual”, Spectral Sciences Inc., Burlington, MA; Air Force Research Laboratory, Hanscom, MA (2008).
[RD08]	Crist, E. P., and Cicone, R. C., "A physically-based transformation of Thematic Mapper data - the Tasseled Cap", IEEE TGRS, Vol. GE-22, 256-263 (1984).
[RD09]	Dozier, J., Bruno, J., and Downey, R. C., “A faster solution to the horizon problem”, Computers & Geosciences, Vol. 7, 145-151 (1981).
[RD10]	Gao, B.-C., and Goetz, A.F.H., “Determination of total column water vapor in the atmosphere at high spatial resolution AVIRIS data using spectral curve fitting and band rationing techniques”, Proc. SPIE, Vol. 1298, 138-150, 1990.

Reference ID and Document Title	
[RD11]	Gao, B.-C., Kaufman, Y.J., Han, W., and Wiscombe, W. J., “Correction of thin cirrus path radiances in the 0.4 – 1.9 µm spectral region using the sensitive 1.375 µm cirrus detecting channel”, J. Geophys. Res., Vol 103, D24, 32,169-32,176 (1998).
[RD12]	Gao, B.-C., Yang, P., Han, W., Li, R.-R., and Wiscombe, W. J., “An algorithm using visible and 1.38 µm channels to retrieve cirrus cloud reflectances from aircraft and satellite data”, IEEE TGRS, Vol. 40, 1659-1668 (2002).
[RD13]	Gao, B.-C., Meyer, K., and Yang, P., “A new concept on remote sensing of cirrus optical depth and effective ice particle size using strong water vapor absorption channels near 1.38 and 1.88 µm”, IEEE TGRS, Vol. 42, 1891-1899 (2004).
[RD14]	Gomez-Chova, L., Camps-Valls, G., Calpe-Maravilla, J., Guanter, L., and Moreno, J., “Cloud-screening algorithm for ENVISAT/MERIS multispectral images”, IEEE TGRS Vol. 45, 4105-4118.
[RD15]	Guanter, L., Richter, R., and Kaufmann, H., “On the application of the MODTRAN4 atmospheric radiative transfer code to optical remote sensing“, Int. J. Remote Sensing, Vol. 30, 1407-1424 (2009).
[RD16]	Hay, J. E., and McKay, D. C., “Estimating solar irradiance on inclined surfaces: a review and assessment of methodologies”, Int. J. Solar Energy, Vol. 3, 203-240 (1985).
[RD17]	Irish, R.R., Barker, J. L., Goward, S. N., and Arvidson, T., ”Characterization of the Landsat-7 ETM+ automated cloud-cover assessment (ACCA) algorithm” Photogr. Engin. Remote Sens. Vol. 72, 1179-1188 (2006).
[RD18]	Kaufman, Y. J., et al. "The MODIS 2.1 µm channel – correlation with visible reflectance for use in remote sensing of aerosol", IEEE TGRS,, Vol. 35, 1286-1298 (1997).
[RD19]	Liang, S., Fallah-Adl, H., Kalluri, S., Jaja, J., Kaufman, Y. J., and Townshend, J. R. G., ”An operational atmospheric correction algorithm for Landsat Thematic Mapper imagery over the land”, J. Geophys. Res., Vol 102, D14, 17,173-17,186 (1997).
[RD20]	Marion, R., Remi, M., and Faye, C., “Measuring trace gases in plumes from hyperspectral remotely sensed data”, IEEE TGRS Vol. 42, 854-864 (2004).
[RD21]	Marion, R., Michel, M., and Faye, C., “Atmospheric correction of hyperspectral data over dark surfaces via simulated annealing”, IEEE TGRS, Vol. 44, 1566-1574.
[RD22]	Nicodemus, F. E., "Reflectance nomenclature and directional reflectance and emissivity", Applied Optics, Vol. 9, 1474-1475 (1970).
[RD23]	Richter, R., “A fast atmospheric correction algorithm applied to Landsat TM images”, Int. J. Remote Sensing, Vol. 11, 159-166 (1990).
[RD24]	Richter, R., "Atmospheric correction of satellite data with haze removal including a haze/clear transition region", Computers & Geosciences, Vol. 22, 675-681 (1996).
[RD25]	Richter, R., “Correction of satellite imagery over mountainous terrain”, Applied Optics, Vol. 37, 4004-4015 (1998).
[RD26]	Richter, R., and Müller, A., “De-shadowing of satellite / airborne imagery“, Int. J. Remote Sensing, Vol. 26, 3137-3148 (2005).
[RD27]	Richter, R., and Schläpfer, D., “Considerations on water vapor and surface reflectance retrievals for a spaceborne imaging spectrometer“, IEEE TGRS, Vol. 46, 1958-1966 (2008).
[RD28]	Richter, R., Kellenberger, T., and Kaufmann, H., “Comparison of topographic correction methods“, Remote Sensing, Vol. 1, 184-196 (2009).
[RD29]	Schläpfer, D., Borel, C. C., Keller, J., and Itten, K. I., “Atmospheric precorrected differential absorption technique to retrieve columnar water vapor”, Remote Sensing of Environment, Vol. 65, 353-366 (1998).
[RD30]	Simpson, J. J., and Stitt, J. R., “A procedure of the detection and removal of cloud shadow from AVHRR data over land”, IEEE TGRS, Vol. 36, 880-897 (1998).
[RD31]	Simpson, J. J., Jin, Z., and Stitt, J. R., “Cloud shadow detection under arbitrary viewing

Reference ID and Document Title	
	and illumination conditions", IEEE TGRS, Vol. 38, 972-976 (2000).
[RD32]	Sirguey, P., "Simple correction of multiple reflection effects in rugged terrain", Int. J. Remote Sensing, Vol. 30, 1075-1081 (2009).
[RD33]	P. Yang, K. N. Liou, K. Wyser, and D. Mitchell, "Parametrization of the scattering and absorption properties of individual ice crystals", J. Geophys. Research, Vol. 105, No. D4, 4699-4718 (2000).
[RD34]	Zhang, Y., Guindon, B., and Cihlar, J., "An image transform to characterize and compensate for spatial variations in thin cloud contamination of Landsat images", Remote Sensing of Environment, Vol. 82, 173-187 (2002).
[RD35]	Chylek, P., Borel, C. C., Clodius, W., Pope, P. A., and Rodger, A. P., "Satellite-based columnar water vapor retrieval with the multi-spectral Thermal Imager (MTI)", IEEE TGRS, Vol. 41, 2767-2770 (2003).
[RD36]	Mouroulis, P., Green, R. O., and Chrien, T. G., "Desing of pushbroom imaging spectrometers for optimum recovery of spectroscopic and spatial information", Applied Optics, Vol. 39, 2210-2220 (2000).
[RD37]	Goetz, A. F. H, Kindel, B. C., Ferri, M., and Qu, Z., "HATCH: results from simulated radiances, AVIRIS, and Hyperion", IEEE TGRS, Vol. 41, 1215-1221 (2003).
[RD38]	Stamnes, K., Tsay, S. C., Wiscombe, W. J., and Jayaweera, K., "Numerically stable algorithm for discrete-ordinate method radiative transfer in multiple scattering and emitting layered media", Applied Optics, Vol. 27, 2502-2509 (1988).
[RD39]	Isaacs, R. G., Wang, W. C., Worsham, R. D., and Goldberg, S., "Multiple scattering LOWTRAN and FASCODE models", Applied Optics, Vol. 26, 1272-1281 (1987).
[RD40]	M. Bachmann, S. Adar, E. Ben-Dor, J. Biesemans, M. Grant, J. Hanus, G. Heuvelink, S. Holzwarth, A. Hueni, E. Knaeps, M. Kneubuehler, K. Meuleman, E. de Miguel, A. Pimstein, E. Prado, I. Reusen, T. Ruhtz and M. Schaale, "DJ2.2.1 - Generic Quality Indicators and Quality Layers," EUFAR FP7, JRA2 - HYQUAPRO, 2010.
[RD41]	M. Bachmann, S. Adar, E. Ben-Dor, J. Biesemans, X. Briottet, M. Grant, J. Hanus, G. Heuvelink, S. Holzwarth, A. Hueni, M. Kneubuehler, K. Meuleman, E. de Miguel, I. Perez Gonzalez, I. Reusen, R. Richter, T. Ruhtz, M. Schaale and S. Weide, "DJ2.2.2 - Quality Layers for VITO, DLR, INTA, and PML," EUFAR FP7, JRA2 - HYQUAPRO, 2011.
[RD42]	M. Bachmann, S. Adar, E. Ben-Dor, J. Biesemans, X. Briottet, M. Grant, J. Hanus, G. Heuvelink, S. Holzwarth, A. Hueni, M. Kneubuehler, K. Meuleman, E. de Miguel, I. Perez Gonzalez, I. Reusen, R. Richter, T. Ruhtz, M. Schaale and S. Weide, "DJ2.2.3 - Quality Layers for USBE,TAU-BarKal;FUB," EUFAR FP7,JRA2 - HYQUAPRO, 2011.
[RD43]	R. Reulke and H. Weichelt, "SNR Estimation of the RapidEye Space-borne Cameras," PFG - Photogrammetrie Fernerkundung Geoinformation, no. 1, pp. 29-38, 2012.
[RD44]	P.D. Noerdlinger, "Atmospheric refraction effects in Earth remote sensing," ISPRS Journal of Photogrammetry and Remote Sensing, vol. 54, no. 5–6, pp. 360–373, Dec. 1999.
[RD45]	Lehner M. and Gill R.S. (1992): Semi-automatic derivation of digital elevation models from stereoscopic 3-line scanner data, IAPRS, Vol. 29, Part B4, Washington, USA, pp. 68-75.
[RD46]	Roth, A.; Knöpfle, W.; Strunz, G.; Lehner, M.; Reinartz, P. (2002): "Towards a Global Elevation Product: Combination of Multi-Source Digital Elevation Models", Symposium on Geospatial Theory, Processing and Applications, Ottawa, 2002
[RD47]	NASA JPL, "ASTER Global Digital Elevation Model." NASA JPL, 2009. https://lpdaac.usgs.gov/dataset_discovery/aster/aster_products_table/astgtm

Reference ID and Document Title	
[RD48]	IERS Conventions (2010), IERS Technical Note No. 36 ftp://tai.bipm.org/iers/conv2010/tn36.pdf
[RD49]	A. Annoni, C. Luzet, E.Gubler and J. Ihde. Map Projections of Europe.; European Commission , JRC; 2003 http://www.ec-gis.org/sdi/publist/pdfs/annoni-etal2003eur.pdf
[RD50]	Coordinate Conversions and Transformations including Formulas; Revised - OGP Surveying and Positioning Guidance Note number 7, part 2 – November2009. http://www.epsg.org/guides/docs/G7-2.pdf
[RD51]	Müller, Rupert und Krauß, Thomas und Schneider, Mathias und Reinartz, Peter (2012) Automated Georeferencing of Optical Satellite Data with Integrated Sensor Model Improvement. Photogrammetric Engineering and Remote Sensing (PE&RS), 78 (1), Seiten 61-74. American Society for Photogrammetry and Remote Sensing. ISSN 0099-1112
[RD52]	Schwind, Peter und d'Angelo, Pablo (2015) Evaluating the applicability of BRISK for the geometric registration of remote sensing images. Remote Sensing Letters, 6 (9), Seiten 677-686. Taylor & Francis. DOI: 10.1080/2150704X.2015.1058986 ISSN 2150-704X
[RD53]	Schwind, Peter (2008) Critical Evaluation of the SIFT Operator for Remote Sensing Imagery. Diplomarbeit, FH Landshut
[RD54]	Wan, Z., Hook, S., Hulley, G. (2015). MYD11A2 MODIS/Aqua Land Surface Temperature/Emissivity 8-Day L3 Global 1km SIN Grid V006. DOI:10.5067/MODIS/MYD11A2.006
[RD55]	Fontenla, J.M., Harder, J., Livingston, W., Snow, M. and Woods, T. (2011). High-resolution solar spectral irradiance from extreme ultraviolet for far infrared. DOI:10.1029/2011JD016032
[RD56]	Richter, R., Schlaepfer, D., Mueller, A (2006), An automatic atmospheric correction algorithm for visible/NIR imagery. DOI: 10.1080/01431160500486690

Table 2-2 Reference Documents

3. Terms and Abbreviations

Terms, definitions, and abbreviations for the DESIS-PAV ground segment are collected in [AD07].

3.1 Definition and indexing of an image cube

Within this document the following understanding of terms will be used:

Let $i, j, k \in \mathrm{N}$ be the natural number indices representing coordinates in 3D space (spatial-spatial-spectral), which are mapped to special physical meanings like digital number $DN_{i,j,k}$, radiance $L_{i,j,k}$ or reflectance $r_{i,j,k}$, with the following definitions

$\boldsymbol{i}$ is the spatial coordinate defined by consecutive sensor exposures increasing with time $\boldsymbol{t}$, also called along track direction.[1]

$\boldsymbol{j}$ is the spatial coordinate defined by the timely read out sequence of a row or sensor line (physical numbering), also called across track direction. It is noted that the definition of the direction and origin can be changed depending on the definition of the coordinate frame.

$\boldsymbol{k}$ is the spectral coordinate increasing from lower to higher wavelengths.

[1] It shall be noted that the DESIS instrument has a rolling shutter. This means that every spectral channel in a frame i is acquired at a sligtly different time. Neverthless, if not other stated, the acquisition time of one spectral channel $\boldsymbol{k}$ is taken as an acquisition time of the entire frame. The number of this spectral channel is defined in 5.2 Raw Data and Virtual Channel. For more details on rolling shutter see section 6.7

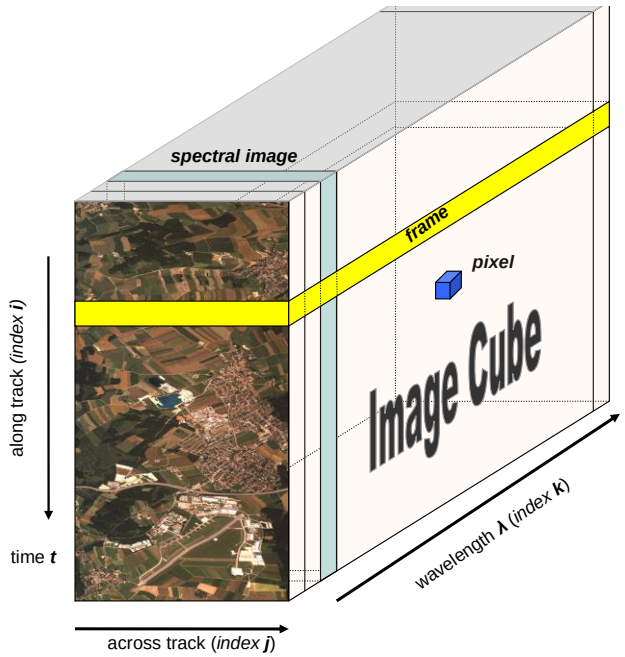

Figure 3-1 HSI image cube and indexing

The spaces and sub-spaces of an image cube are defined in Table 3-1 and represented in Figure 3-1.

Space	Definition	Identifier	Synonyms	Comment
3-dimensional	all i, j, k are variable	image cube	• cube • volumetric image • image	
2-dimensional	i is fixed j, k are variable	frame	• read out • frame read out	
	k is fixed i, j are variable	spectral image	• channel • spectral channel • channel file • band	A virtual channel contains additional information
	j is fixed i, k are variable			No practical usage
1-dimensional	i is variable j, k are fixed	column		
	j is variable i, k are fixed	row	• sensor line • read out index ROI • scan line • line	The ROI defines the actual transferred data
	k is variable i, j are fixed	spectral pixel vector	• spectrum • pixel vector	

Space	Definition	Identifier	Synonyms	Comment
0-dimensional	$\boldsymbol{i}, \boldsymbol{j}, \boldsymbol{k}$ are fixed	pixel	• sample • voxel	Smallest unit, which can be addressed. Often used as entity.

Table 3-1 Spaces and sub-spaces of an image cube.

4. Processor Overview

This section gives a brief overview of the proposed processing chain for DESIS hyperspectral optical data.

The processing chain for DESIS hyperspectral optical data consists of the following four modules which apply non-trivial algorithms (the module code is given in brackets):

• Transcription Processor for DESIS image data and DESIS calibration measurement data (DESIS_HSI_L1A): This processor derives data from the different data streams (image data, calibration measurement data, AOCS data) and prepares these data for long term storage. L1A products are not delivered to the user.

• Systematic and Radiometric Correction Processor for DESIS image data (DESIS_HSI_L1B): This processor corrects the data for known systematic effects and converts these data to physical Top-of-Atmosphere (TOA) radiance values. L1B products are described in [AD01] .

• Geometric Correction Processor for DESIS image (DESIS_HSI_L1C): This processor generates orthorectified images using direct georeferencing with an accurate digital elevation model. L1B products are described in [AD01].

• Atmospheric Correction Processor for DESIS image data (DESIS_HSI_L2A): This processor generates aerosol optical thickness information and surface reflectance images, namely Bottom-of-Atmosphere (BOA) radiance values. L2A products are described in [AD01].

The following illustrates which processors and products can be generated by the DESIS processing chain

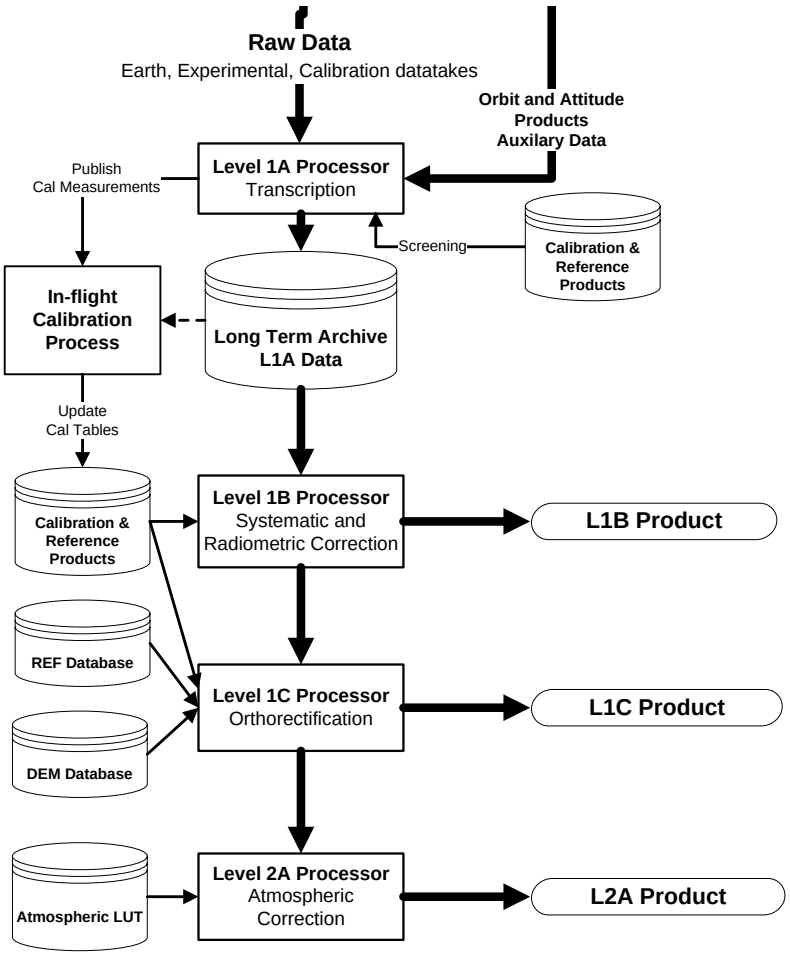

Figure 4-1 Processing Overview and Product Tree

5. Transcription Processor L1A

The Level 1A Processor, which mainly collects information from the different data streams, extracts and interprets information, and evaluates and derives additional information, creating the Level 1A Products from Earth data and Calibration data measurements. The L1A Experimental Mode Products are generated from forward motion compensation mode data and global shutter data with an along track spatial resolution of 60 m by the L1A Processor. The functionality of the L1A Processor for Experimental Mode Products is limited. During the L1A processing no data manipulation (change) is performed, thus the process is reversible and it is possible to fully reconstruct raw data. Figure 5-1 shows the overview of the L1A processor.

L1A Earth Product, L1A Calibration Product and L1A DC product generated by the L1A processor are stored in a long term archive and are not delivered to the user.

The L1A Experimental Mode Products are stored in a long term archive, delivered to (special) users, but no further processing is carried out. For the stereo mode data takes there is an exception in higher level processing, because they are processed towards L1B, L1C and L2A (similar as the so called Earth data takes), but no specific stereo processing is applied.

5.1 Overview

The functionality of the Level 1A Processor can be distinguished into transcription, screening and quality assessment tasks. The raw data are not compressed. It is assumed that the data from task order and the data from catalogue order have the same format.

Transcription and screening tasks include:

- Screening of Virtual Channel (VC) and raw data
- Extraction and evaluation of Dark Current (DC) measurements
- Preparation of Earth Data Takes (EARTH)
- Tiling and reformatting of raw data I
- Processing of Calibration Data Takes (CAL)

Quality assessment tasks include:

- Screening of raw data
- Dead pixel mask

To derive quality and catalogue information, e.g. quicklooks, L1A Processing includes also some functionality of the L1B Processor. L1A Processing of Experimental Mode data takes is limited to the storing of the L1A Experimental Mode Products and corresponding data from other data streams.

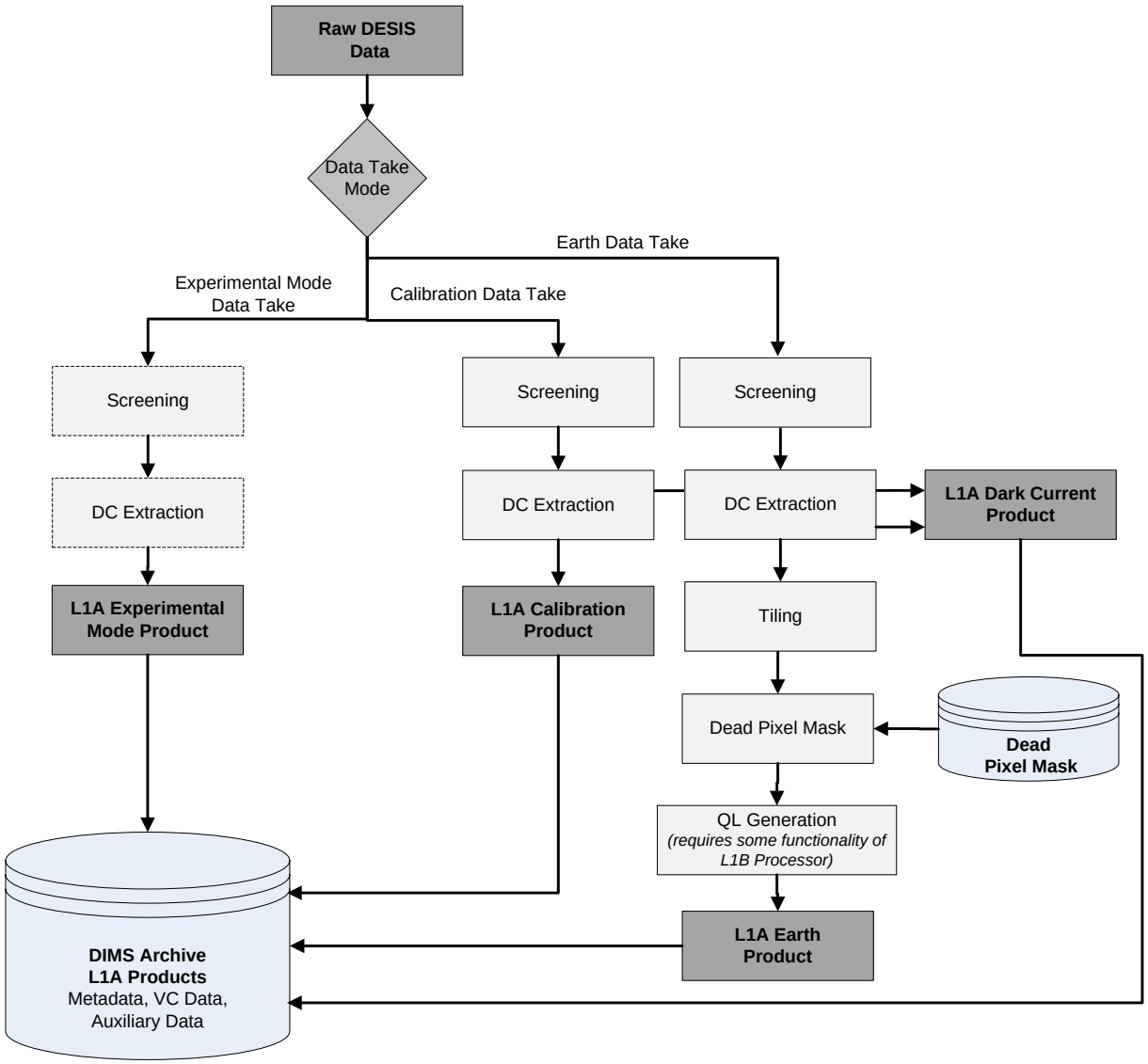

Figure 5-1 Overview of the Transcription Processor L1A. Three different modes of raw DESIS Data are processed by the L1A Processor, these are: Earth Data Take, Calibration Data Take and Experimental Mode Data Take. The outputs of the L1A processor are L1A Earth Product, L1A Calibration Product, L1A Dark Current Product and L1A Experimental Mode Product, which are all archived in the corresponding long term archive. Additionally, metadata, virtual channel data and other axillary data are also stored as a part of the products.

5.2 Raw Data and Virtual Channel

The DESIS raw data are acquired as an array of frames. Each frame has identical dimensions $(N\boldsymbol{k}+\boldsymbol{2})\times N\boldsymbol{j}$, and consists of 2 Virtual Channels (VC) and a Spectral Image (SI). The structure of Frames is the same for Earth Data Takes (DT) and DC DT.

The index $\boldsymbol{i}$ defines a time direction (along track). The length $N\boldsymbol{i}$ (number of frames) depends on the length of a DT and is a multiple of 1024, i.e. $1024 \times N$. Due to a rolling shutter, each spectral channel of one frame is read out after the previous, i.e. at a slightly different time. Therefore, the acquisition time of the whole frame refers to the acquisition time of the spectral channel when the FSync pulse is sent [AD10]. The time offset between the first spectral channel (row) and the Fsync trigger is written in the VC [AD11]. The DESIS sensor has the top and

the bottom detector, which behave identically according to the timing of the readout. The rows are readout in the opposite direction, i.e. the first row and the last row of the top and bottom detector, respectively are readout at the same time. See [AD11] for details.

- The index $\boldsymbol{j}$ defines a spatial direction (across track). The length $N\boldsymbol{j}$ is 1024 pixels.
- The index $\boldsymbol{k}$ defines a spectral direction. The length $N\boldsymbol{k}$ is 235 SI, with additional 2 VC

The file format of the data generated by the DESIS instrument is defined in [AD03]. The VC is separated from SI, and stored in the archive as a part of the L1A Earth or L1A Calibration Product.

5.3 Screening

The screening of the data performs a first inspection of all status information, temperatures, which are available in the virtual channel (VC) of the DESIS instrument data. This procedure is part of the L1A processor and has to be executed for each input raw data set at first to ensure that the instrument works well and all parameters are within the normal working range. The working range has to be defined from the space segment [AD12] and is the range in which the instrument is expected to be work correctly.

Additionally, the screening checks the measured dark values before and after earth observation or calibration if they are in the defined range in comparison to reference dark values.

The screening procedure includes following steps:

- Cyclic redundancy check (CRC)
- Temperature check
- Check of dark values
- Instrument operational parameter inspection

Input data	**Output data**	**Auxiliary data**	
		Before Launch	After Launch
• Raw DESIS data	• screened Raw DESIS data • Logfile • Quality status flag	• Preliminary list of defined parameters to be checked • Preliminary table of transfer functions, nominal values and bounds for each parameter	• Confirmed list of defined parameters to be checked • Confirmed table of transfer functions, nominal values and bounds for each parameter

Table 5-1 Parameters of Screening

The test procedures of temperatures comprise a defined basic set of the most important parameters. This fixed set can be extended by definition of extra parameters and their reference values and bounds.

The screening procedure does not change the raw DESIS data set, but adds information about the test results to dedicated attributes in the metadata.

The result of the overall screening procedure is a quality status flag named screeningStatus that is set as follows:

- 1 = FAULTLESS/OK, if all checks were successfully passed
- -1 = WARNING, if minor errors have occurred
- 0 = ERROR, if at least one check has failed with a major error

```
<screeningStatus>1</screeningStatus>
```

If the screening procedure has detected an error (dark measurement cycle is missed, reference bounds or thresholds of an examined parameter were exceeded) then a quality flag statement is set (short explanation about the reason of failure) and a message is written to the log file.

The log file contains information about all performed checks and their return value.

5.3.1 Temperatures

The following temperature values are screened and compared to pre-defined value ranges [see [AD12]]

ICU Temperature 0 - POI Box
ICU Temperature 1 - ICU Box
ICU Temperature 2 - POI Motor
ICU Temperature 3 - PCHU box
ICU Temperature 4 - Radiator SA
ICU Temperature 5 - FEE Box
ICU Temperature 6 - SA TEC
ICU Temperature 7 - Fix Mirror 2
ICU Temperature 8 - Fix Mirror 1
ICU Temperature 9 - TMA structure
ICU Temperature 10 - TMA structure
ICU Temperature 11 - instrument panel
ICU Temperature 12 - Offner mirror
ICU Temperature 13 - Offner structure
ICU Temperature 14 - LED 1
ICU Temperature 15 - LED 2

The mean value and standard deviation over the whole data take will be calculated:

$$\overline{T}_i = \frac{1}{n}\sum_{k=1}^{n} T_{i,k} \qquad (5\text{-}1)$$

$$\sigma_i = \sqrt{\frac{1}{n}\sum_{k=1}^{n}(T_{i,k} - \overline{T}_i)^2}$$

for each selected temperature T_i (i = number of the investigated temperature sensor, n = number of frames collected during one monitor cycle).

It will be checked, whether the mean value of all relevant temperatures is within the required operational range

$$temp_i^{\min} \le \overline{T}_i \le temp_i^{\max} \qquad (5\text{-}2)$$

and whether 90% of all values $T_{i,k}$ are within the interval

$$\overline{T_i} - 2\sigma \le T_{i,k} \le \overline{T_i} + 2\sigma \qquad (5\text{-}3)$$

$temp_i^{\min}$ and $temp_i^{\max}$ are individual limits for each temperature sensor.

If for all temperatures conditions are fulfilled, then the test for temperatures is positive and a status variable of type integer is set accordingly.

The positive test result is written to the log file. For temperatures outside the specified limit, an additional note is written to the log file. This approach tests whether the measured temperatures behave in a normally expected statistical manner. Each temperature sensor is described in its own parameter block in the metadata. This block contains name, description, type, value, units, and the status result (1 for OK, -1 for WARNING, 0 for ERROR). If an error was found, explanatory information on the cause is provided as additional information. The framed box contains an example.

```
<qualityIndicator>
    <screeningResult>
        <parameter>
            <status>0</status>
            <name>FPAVL.xHKInterfaceSaT1.u16iT1CisPT1000</name>
            <type>temperature</type>
            <description>FPA SA detector temperature T1 (PT1000 sensor)</description>
            <info>Overflow of operating limit</info>
            <value>56.3</value>
            <units>degC</units>
        </parameter>
    </screeningResult>
</qualityIndicator>
```

5.3.2 CRC

The following CRC (Cyclic Redundancy Check) values of the data and data header files are checked

CRC Check File Fixed Header

CRC Check File Mode Header

CRC Check Session Fixed Header

CRC Check Session Mode Header

CRC Check Frame Mass Memory Top

CRC Check Frame Mass Memory Bottom

5.3.3 Dark current screening

The dark current before and after each data take are measured in 100 frames each for low gain and high gain [AD09] for noise reduction in the measurement data. Mean values and standard deviations are

calculated for each dark measurement sequence. The mean dark values (before and after) of each data take will be checked, whether they do differ of more than a certain value from the reference values. The reference and threshold values will be defined pre-launch from laboratory calibration evaluation and their statistical analysis. Therefore, the mean dark values will be checked against their references as follows:

$$\overline{Diff}_{j,k}^{dark} = abs(\overline{DN}_{j,k}^{dark} - DN_{j,k}^{dark\_ref}) \leq ref^{dark} \quad \textbf{(5-4)}$$

where

$\overline{DN}_{j,k}^{dark}$ is the mean value of dark measurement of spatial pixel j and spectral channel k before

$DN_{j,k}^{dark\_ref}$ reference value for dark measurement of spatial pixel j and spectral channel k before

ref^{dark} threshold value

Threshold values are defined in [AD04].

This procedure will be carried out for the dark value measurements before and after each earth or calibration measurement. The test result will be written in the metadata file (parameter status: -1 for WARNING, 0 for ERROR, 1 for FAULTLESS/OK).

The dark current measurements are stored in the L1A DC product DESIS.HSI.DC [AD04]. The framed box contains an example of the DC quality indicator in the metadata file.

```
<qualityIndicator>
        <darkBeforeQuality>
                <available>true</available>
                <status>1</status>
        </darkBeforeQuality>
        <darkAfterQuality>
                <available>false</available>
                <status>0</status>
        </darkAfterQuality>
</qualityIndicator>
```

5.3.4 Instrument Operational Parameters Metadata

The virtual channel [AD03] contains a set of parameters giving the operational work status of the instrument. A defined subset of the most important parameters has to be inspected to ensure that the instrument commands were correctly carried out and the operational modes are properly set.

5.4 Earth Data

This chapter describes the preparation steps of the Earth DT. The Earth data are stored as a L1A Earth Product, which contains data from Earth image scene after tiling. The data are in Band Interleaved by Line (BIL) format [AD03] for ingestion in the DIMS archive. The Earth Product definition is available in [AD04]. The processing of the Earth DT includes

- Dark Current extraction
- Tiling of the (unpacked) raw DESIS data
- Dead pixel mask

- Quicklook generation
- Metadata generation for product creation.

Input data	Output data	Auxiliary data	
		Before Launch	After Launch
• Raw Earth DESIS data separated in SI and VC data • MUSES Auxiliary Data (trajectory files)	• L1A Earth Product divided into N tiles • L1A DC Product	• Dead Pixel Mask (from Calibration Tables)	

Table 5-2 Parameters of Earth Data Processing

5.4.1 Dark current extraction

Dark current (DC) measurements before DT acquisition and after DT are extracted for all channels. A separate L1A DC Product (before and after the DT) is created and prepared for ingestion in the DIMS archive. The DC data are stored in the BIL format. The L1A DC data form an array of a size $N\boldsymbol{j}\times n\times N\boldsymbol{k}$, where n is the number of DC Frames before or after the DT acquisition.

Information about POI unit and number of the DC Frames before and after the DT acquisition is stored in one of the two VC channels of every frame. For all n DC frames a cross check will be made, weather the POI position is correct. For the DC Frames after DT acquisition, the same procedure is applied as for the DC Frames after the DT acquisition.

A mean value for each spatial pixel $\boldsymbol{j}$ and each spectral channel $\boldsymbol{k}$ before and after DT acquisition is calculated

$$\overline{DN}_{j,k}^{dark} = \frac{1}{n}\sum_{i=1}^{n} DN_{i,j,k} \qquad (5\text{-}5)$$

where

$\overline{DN}_{j,k}^{dark}$ is the mean value of DC measurements spatial pixel $\boldsymbol{j}$ and spectral channel $\boldsymbol{k}$,

$DN_{i,j,k}$ is a readout value of dark measurements for spatial pixel $\boldsymbol{j}$ and spectral channel $\boldsymbol{k}$, at the time $\boldsymbol{i}$,

n is the number of DC frames before or after the DT acquisition.

A linear interpolation between mean value of DC measurements before and after DT acquisition will be calculated for every frame of the DT acquisition to avoid inaccuracies due to possibly occurring change of dark values that could be caused by temperature drift. The dark current correction for spatial pixel $\boldsymbol{j}$ and spectral channel $\boldsymbol{k}$ for a time t is given by

$$DN(t)_{j,k} = \overline{DN}_{j,k}^{dark\_start} + \frac{\overline{DN}_{j,k}^{dark\_end} - \overline{DN}_{j,k}^{dark\_start}}{t_{end} - t_{start}}(t - t_{start}) \qquad (5\text{-}6)$$

where

t is acquisition time of a frame in a DT,

t_{start}, t_{end} is the time of the first and the last frame in a DT acquisition,

$\overline{DN}_{j,k}^{dark\_start}$, $\overline{DN}_{j,k}^{dark\_end}$ is the mean value of DC measurements spatial pixel $\boldsymbol{j}$ and spectral channel $\boldsymbol{k}$ before and after DT acqusition.

Mean and standard deviation values of the dark current before (start) and after (end) each DT acquisition and the number of DC Frames before and after the DT acquisition are calculated The DC data are prepared for ingestion into DIMS.

5.4.2 Tiling of the DESIS data

After DC extraction, the remaining part of the data is SI DESIS data. They are tiled into images of a size$N\boldsymbol{j}\times(1024+2*8)$. A size of each tile is $(1024+2*8)\times N\boldsymbol{j}\times N\boldsymbol{k}$. An overlap between subsequent tiles of one DT is eight lines. The overlap is required for L1B, L1C, and L2A Processors. The L1B tile delivered to the user is without overlap. The overlap is not removed for L1C and L2A products.

First and last eight lines of the first and last tile in one DT are not available and regarded as background. The background value is set to 2^16-1 (all bit set to one unsigned 16 bit value). In case that the RS mode is used, the frame immediately before the first Earth-image frame of the first tile (only) in a datatake will be filled with a clone of the first Earth-image frame (instead of the background value). This is done to reduce the artifacts on the first RS-corrected Earth-image frame after the RS correction is applied. The pixels in the first row of the first tile in a datatake shall be marked as "abnormal" in the corresponding quality layer of the RS-corrected products.

Only tiles with a full length of 1024 are processed. Maximal length of a DT can result in 100 tiles.

The following parameters will be written on the metadata file: Tile ID, Number of Tiles.

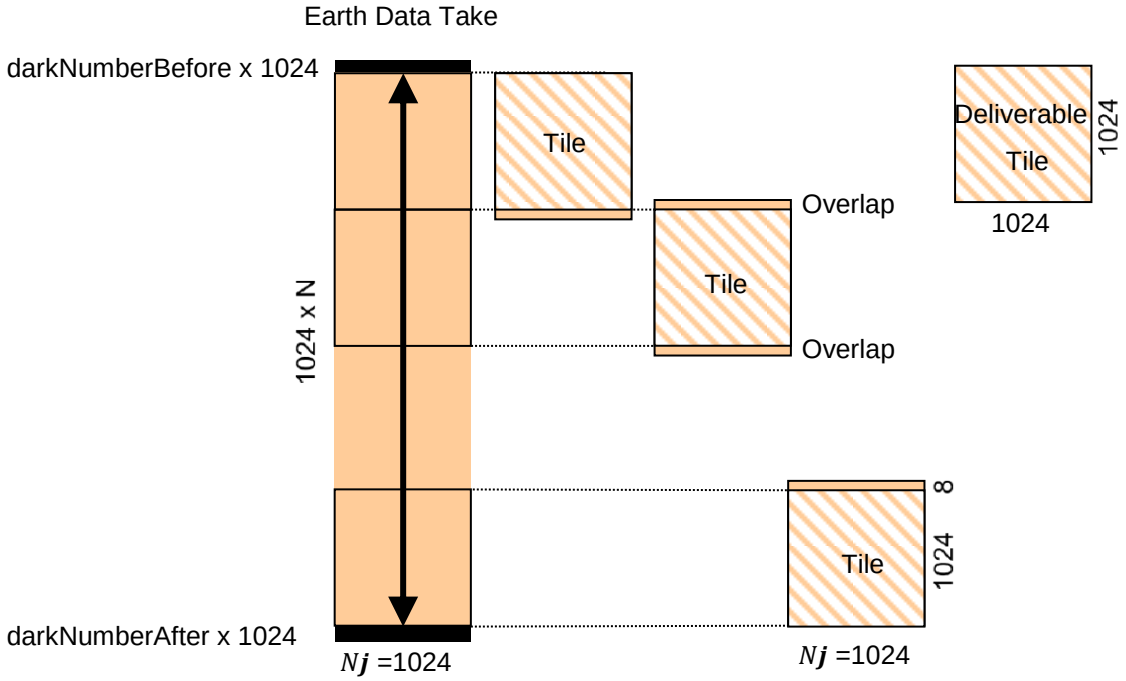

Figure 5-2 Tiling of the DESIS Earth Data Take. First, the DC before and after each Earth DT is extracted. Then, the Spectral Images (SI) is tiled into N tiles with a size $(1024+2*8)\times Nj\times Nk$. There is an 8 lines overlap between subsequent tiles. Tiles delivered to the user are without overlap, and have a size of 1024×1024.

5.4.3 Dead pixel mask

First, the global Dead pixel mask will be loaded within the L1A processor. The Dead pixel mask containing $Nj \times Nk$ is included in the radiometric reference data package. It will be used for marking of permanently dead pixels in the data. The dead pixel mask is a quality layer of the L1A Data Product [AD04].

5.4.4 Quicklook generation

Image quicklook (QL) are generated for each tile separately by some functionalities of the L1B processor. The re-processing of the L1A products is not foreseen. Therefore, a potential inconsistency between the L1A and L1B quality quicklook can occur.

One tile is transformed to 8-bit pixel values and radiometrical adjusted for optimal displaying. For the quicklook generation the following channels will be used: 500nm (blue), 650 nm (red), and 850nm (infrared). The format of the Quicklook is tif [AD04].

5.5 Calibration Measurement Data

The processing of calibration DT is similar to the processing of the Earth DT. However, no tiling of the calibration data is carried out. The radiometric and spectral calibration is carried out by measurements of the dark current before and after each DT and internal light sources (LED). The goal of calibration DT is to characterise the sensor. If changes in spectral and/or radiometric characteristics of the sensor occur, the calibration tables will be updated. Pre-launch spectral and geometric calibration and characterisation of the sensor will be carried out.

5.6 Experimental Products

The functionality of the L1A Processor for Experimental Mode Products is limited. This means that only the raw data are ingested in the DIMS. No dark current extraction, tiling, quicklook generation, screening and quality check of the data are carried out. Exceptions are the Stereo mode data takes, which are processed towards L1B, L1C and L2A (similar to the so called normal Earth data takes), but no specific stereo processing is applied.

If the data format of the Experimental Mode Products is equal to that of the calibration DT or Earth DT, and the Experimental Mode DT contains the same VC information and dark current measurements, then the screening procedure and the dark current extraction can also be executed.

The L1A Experimental Mode Products are delivered to the user. No other L1A products are delivered to the user.

6. Systematic and Radiometric Correction Processor L1B

Development Level 1B Processor corrects the HSI image data for known systematic effects, for instance odd-even, non-linearity, non-uniformity. It also converts the system corrected HSI image digital numbers (DN) to physical at-sensor radiance values based on the currently valid calibration values and dark current (DC) information. Only Earth data takes (DT) are processed by the L1B Processor.

6.1 Overview

The L1B processor uses as an input L1A Product (one tile), which is stored in an archive. The L1B Product is delivered directly to the user and is not stored in the DIMS archive.

6.2 Input

Input data	**Output data**	**Auxiliary data**	
		• Before Launch	After Launch

• L1A Earth Product (one tile)
• L1A DC Product
	• L1B Product	• Dead Pixel Mask
		• Data Packages:
		  ○ Non-Linearity
		  ○ Spectral Calibration
		  ○ Radiometric Calibration
			• Periodic update
			• Update if required

Table 6-1 Parameters for systematic and Radiometric Correction Processor L1B

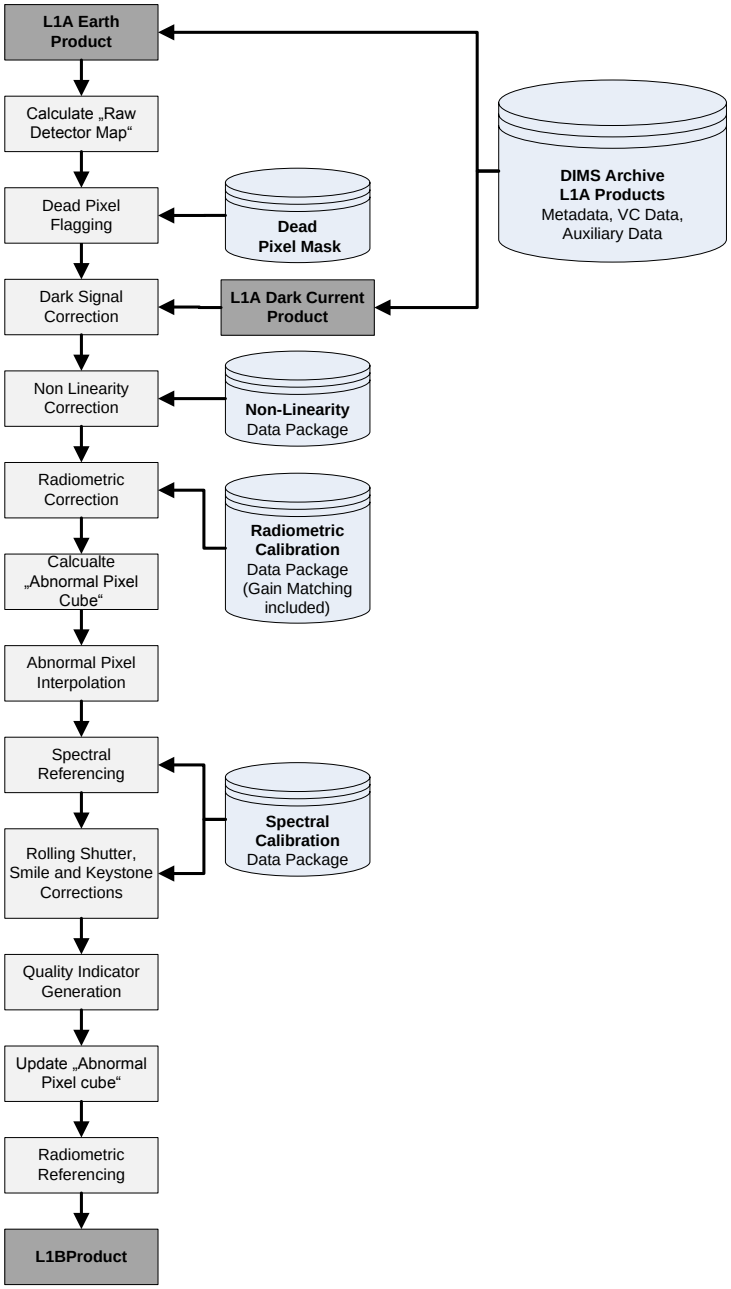

Figure 6-1 Overview of the Systematic and Radiometric Correction Processor L1B

6.3 Processing Algorithm

The L1B processing algorithm is responsible for delivering at sensor radiances from the DN digitised after read out of the focal plan array signal in the DESIS sensor. Assuming that the dead pixels are flagged and not considered for the further processing, the L1B algorithm performs systematic corrections that can be described mathematically in a compact form as

$$L_{j,k} = G_{j,k} \cdot \left(DN_{j,k}^{lin} - \overline{DN}_{j,k}^{dark} \right) \quad (6\text{-}1)$$

where

$L_{j,k}$ is spectral radiance at-sensor,

$G_{j,k}$ is radiometric correction factor,

$\mathrm{DN}_{j,k}^{lin}$ is pixel value corrected for non-linearity (see 6.3.1),

$\overline{\mathrm{DN}}_{j,k}^{dark}$ is pixel's dark signal value (from 5.4.1) corrected for non-linearity (see 6.3.1).

The following chapters describe in detail each of the processing steps.

6.3.1 Non-Linearity Correction

For non-linearity correction a lookup table (LUT) is used

$$DN_{j,k}^{lin} = DN_{j,k} + \delta DN_{j,k}(DN) \quad (6\text{-}2)$$

where

$DN_{j,k}$is a digital number, stored in an L1A product frame

$\delta DN_{j,k}$ is the non-linearity correction value (from Non-Linearity Data Package in [AD04])

6.3.2 Dark Signal Correction

The dark current signal correction is obtained subtracting the values obtained from 5.4.1 which uses DC data taken before and after each data take.

$$DN_{j,k}^{dsc} = DN_{j,k}^{lin} - \overline{DN}_{j,k}^{dark} \quad (6\text{-}3)$$

where

$\overline{\mathrm{DN}}_{j,k}^{dsc}$ is a digital number with the dark signal correction,

$\mathrm{DN}_{j,k}^{lin}$ is a digital number corrected for non-linearity in 6.3.1,

$\overline{\mathrm{DN}}_{j,k}^{dark}$ represents the pixel's dark signal value (from 5.4.1) corrected for non-linearity as in 6.3.1.

6.3.3 Radiometric Correction

In this step the transformation from DN to L radiances is performed applying the radiometric correction factor to the corrected by linearity and dark signal values $DN_{j,k}^{dsc}$. Thus, the radiometric correction is defined as

$$L_{j,k} = G_{j,k} \cdot DN_{j,k}^{dsc} \quad (6\text{-}4)$$

where

$L_{j,k}$ is spectral radiance at-sensor,

$\overline{\mathrm{DN}}_{j,k}^{dsc}$ is a digital number with the dark signal correction from 6.3.2,

$G_{j,k}$ is radiometric correction factor defined as,

$$G_{j,k} = \frac{1}{\frac{Integration\ Time}{118} \cdot Calcoeff_{j,k}}$$

where

$Integration\ Time$ value is readed from the DESIS L1A product metadata file,

$Calcoeff_{j,k}$ is a radiometric coefficient for a nominal integration time stored in the Radiometric coefficient Table, see [AD02].

The DESIS sensor has a low and high gain readings. Therefore, all gain readings have to be taken from the corresponding part of the Radiometric Coefficient Table.

6.4 Quality Indicators Generation

The quality indicators are summarized in Table 6-2 Summary of inputs and outputs in terms of quality indicators

. Quality indicators of a L1B Product are stored in a Geotiff format. See [AD04] for details.

Input data	**Output data**	**Auxiliary data**	
		• Before Launch	After Launch
• Radiance Image-cube (one tile, processed to L1B)	• Abnormal pixels Mask • Abnormal pixels proportions • Detector map • Line mask: 'stripped' • Column mask: 'stripped' • Bad Pixel Mask (see 5.4.3)	• Pixels Saturation Values	• None

Table 6-2 Summary of inputs and outputs in terms of quality indicators

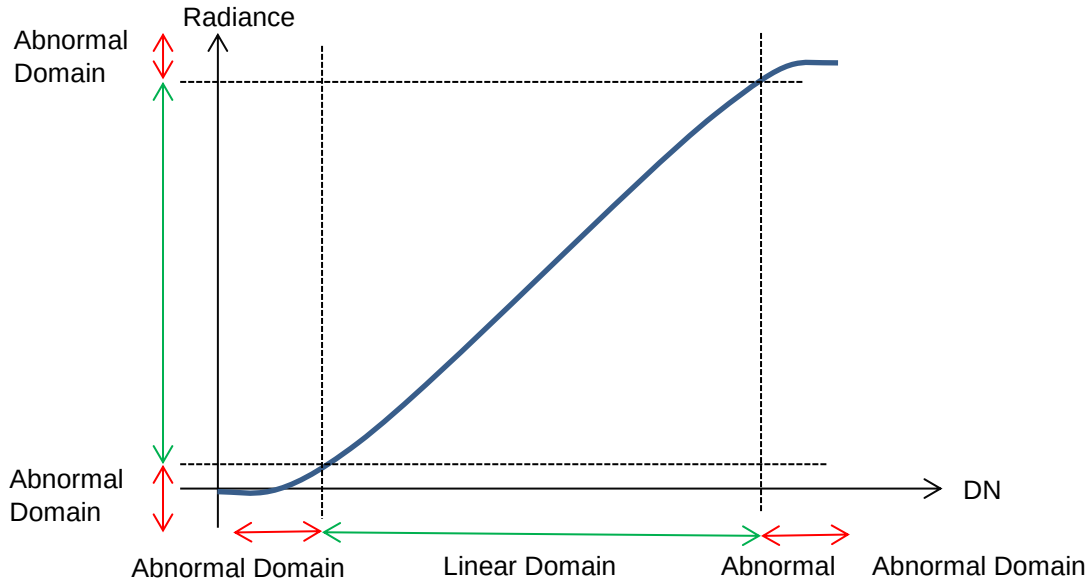

Figure 6-2 Relationship between Abnormal pixels and calibration curve

6.4.1 Analysis for abnormal pixels

Pixels with an abnormally high radiance, i.e. having radiance values above a given (90% [TBD09] of saturation value s) saturation threshold are masked out. Similarly for each band, pixels with radiance below a given threshold (radiance of 1% saturation value [TBD10]) are accounted as 'too low radiances'. As long as these TBDs are not resolved, the conservative thresholds of DN=100 for “too low radiance” and of DN=8000 for “too high radiance” are used based on the analysis of selected L1B scenes during Commissioning Phase.Their proportion as well as their spatial coordinates is returned in form of an image-mask [RD40], [RD41], [RD42]: the so-called abnormal pixels mask. The abnormal pixel mask is one of the quality layers of the L1B Data Product [AD04] and is defined as the union of masks MS and MN respectively which are also saved as quality layers

$$\forall\, i,j\colon MS_{i,j} = \mathrm{Card}(\{k \mid L_{i,j,k} > 0.9s\}) \qquad (6\text{-}5)$$

$$\forall\, i,j:\ MN_{i,j} = \mathrm{Card}(\{k \mid L_{i,j,k} < 0.01s\})$$

6.4.2 Calculation of the detector maps

Regarding data properties related to radiometric calibration and the stability of calibration, there is the necessity for an operational check since the correctness of radiometry is most essential [RD40][RD41][RD42]

Calculation of average spectral radiance and standard deviation separately for every image column of the whole image tile

$$\bar{L}(j,k) = \frac{1}{n}\sum_{a=1}^{n} L(i_a, j, k)$$

$$\sigma L(j,k) = \sqrt{\frac{1}{n}\sum_{a=1}^{n}(L(i_a, j, k) - \bar{L}(j,k))^2}$$

Where

$\bar{L}(j,k)$: mean radiance value for image column j in band k over all scan lines i

$\sigma L(j,k)$: standard deviation of radiance values for image column j in band k over all scan lines i

n: total number of scan lines of the image

The resulting bandwise column mean matrix is denoted “Detector Map”, as each element of this matrix represents one detector element of the chip Figure 6-3 . Thus the detector has the dimensions of j spatial pixels by k spectral pixels. This detector map is stored as part of the quality mask. Note that the standard deviation matrix is only used internally and is not part of the L1B product.

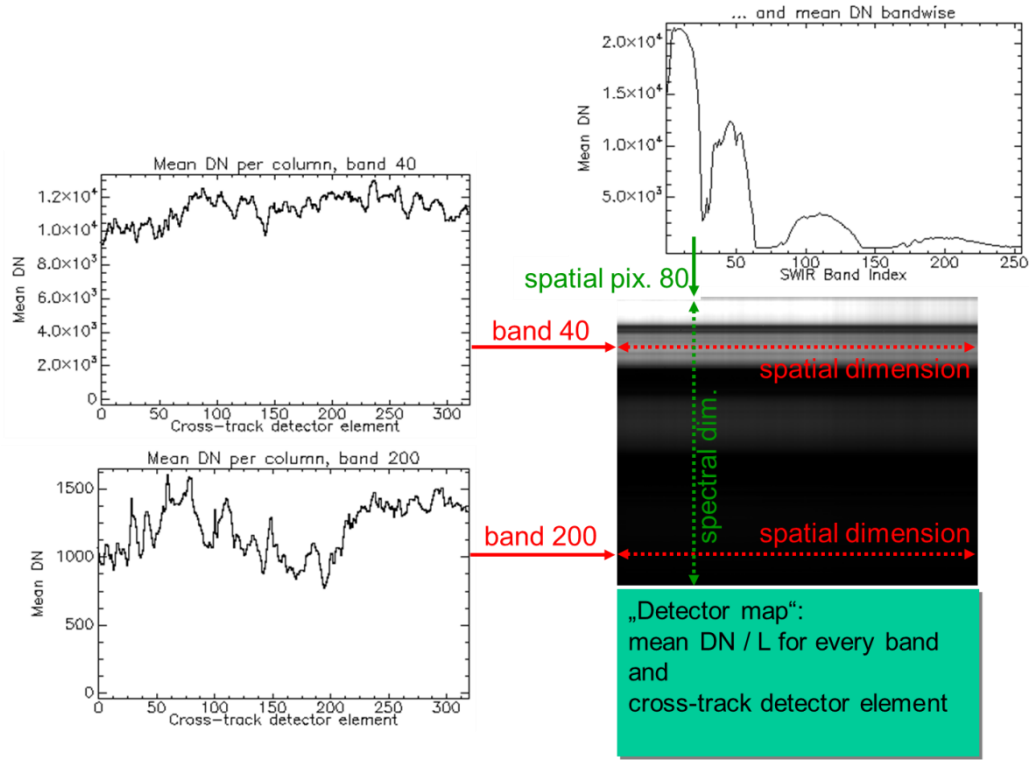

Figure 6-3 Schematic concept of the detector map (example based on HySpex SWIR data).

6.4.3 Analysis for stripping and banding

The analysis of striping and banding artefacts is based on the calibrated detector map, and contributes to the Data Quality Quicklook of the DESIS L1B/L1C/L2A products [AD04]. The approach consists of 3 steps:

1) Test if scene is useful for additional automated analysis, i.e. assumption on scene statistics and homogeneity is valid.

The first criterion is a “sanity check” that the median radiance (i.e., the median of the detector map) is within a given range, so that abnormal scenes having a too high or too low radiance are excluded.

$$threshold_{low} > \bar{L}_{scene} > threshold_{high}$$

Based on selected L1B scenes acquired during Commissioning Phase, these thresholds are set to DN=500 and DN=1200 respectively.

The second criterion is that for each band the sum of absolute differences to the bandwise median is smaller than a given threshold of DN=100.

$$\sum abs(L_{DM}(j,k) - \bar{L}_{DM}(k)) < threshold$$

With $L_{DM}(j,k)$ being the radiance value of the detector map for cross-track element j in band k, and $\bar{L}_{DM}(k)$ being the mean radiance value of the detector map in band k.

If the absolute difference to the mean is high, then the scene is likely heterogeneous, which renders the subsequent analysis meaningless and such analysis is skipped. Thus the automated test triggers the following QC processing.

2) Analysis for striping:

If the radiometric response of a detector element is slightly different in relation to the spatially adjacent detectors (i.e., as caused by incorrect or instable gain and offset values), the corresponding column in the affected image band appears brighter or darker than the adjacent columns. Other causes of striping include dirt on a detector element, or shift of the entrance slit in-flight relative to the in-lab characterization resulting in a not fitting response matrix. For all the mentioned causes, from a data processing point of view, a single striping column thus has a higher or lower average radiance when compared to adjacent columns.

Therefore an automated check can be based on the radiance detector map. An illustrated example using airborne hyperspectral data from the HySpex pushbroom scanner is given in **Fehler! Verweisquelle konnte nicht gefunden werden.**. On the left of the illustration the detector map is depicted, as well as a zoom on the dubious detector element which is related to band 31, cross-track pixel 237. This de-calibrated detector element has a difference of ~30% in radiance to the spatially and spectrally neighbouring elements of the detector map. On the top-right, a subset of the HySpex scene in band 31 is given, which shows a striping artefact in column 237. On the bottom-right the cross-track radiance profile in band 31 is given for one line providing an indication of the absolute magnitude of the striping.

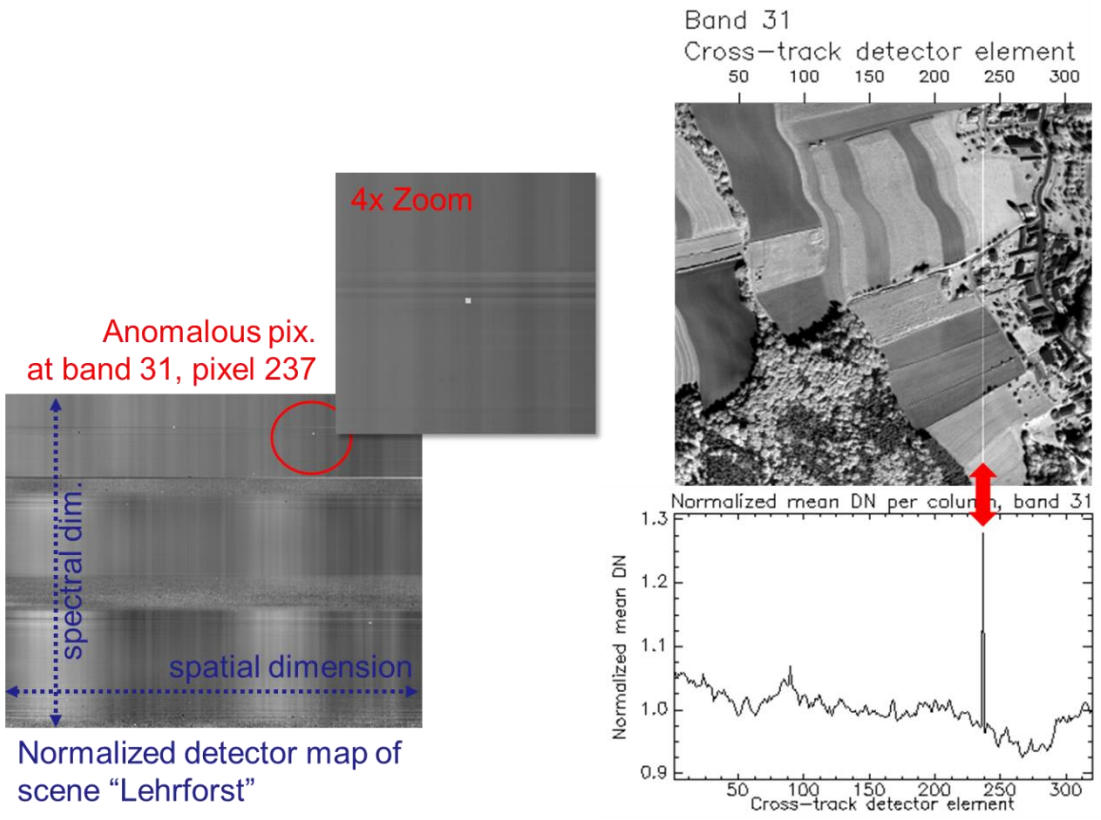

Figure 6-4 Example using HySpex data for the detection of striping and the de-calibrated detector elements causing striping. On the left: normalized detector map of a single HySpex SWIR scene, incl. zoom on the detector element in question. Top-right: part of the HySpex image of band 31; bottom-right: cross-track radiance profile of band 31.

.

In order to detect such decalibrated detector elements, thresholds based on absolute difference of DN=200 in spatial direction and of DN=180 in spectral direction in radiance units can be used:

$$L_{DM}(j,k) - 0.5*(L_{DM}(j-1,k) + L_{DM}(j+1,k)) > threshold \qquad (spatial\ direction)$$
$$L_{DM}(j,k) - 0.5*(L_{DM}(j,k-1) + L_{DM}(j,k+1)) > threshold \qquad (spectral\ direction)$$

$$\sigma L_{DM}(j,k) - 0.5*(\sigma L_{DM}(j-1,k) + \sigma L_{DM}(i+1,k)) > threshold \qquad (spatial\ direction)$$
$$\sigma L_{DM}(j,k) - 0.5*(\sigma L_{DM}(j,k-1) + \sigma L_{DM}(i,k+1)) > threshold \qquad (spectral\ direction)$$

This automated analysis is done for all bands without strong atmospheric absorptions and having a nominal signal-to-noise performance, so consequently not all bands k are used.

For the analysis of pixels which are saturated or generate no significant signal, the results of this test are compared to the defective pixel flagging carried out by calibration/screening. The main difference is that as the described additional tests are carried out on fully calibrated and processed data, while the defective pixel screening is carried out on raw DN before calibration. So it is expected that differences between these two masks occur, as the flagging on DN level is used for the instrument monitoring, and the later flagging is used to describe and to flag the calibrated L1B data set.

Regarding subsequent interactive procedures, the analysis of multiple detector maps can be used to check for consistently decalibrated pixels. An illustration is given in Fig. 6.5, where the mean detector map

of 82 HySpex SWIR datasets is depicted (left part). The detector element corresponding to pixel 237, band 31 shows the anomalous behaviour in all these 82 datasets, thus it can be expected that the decalibration problem is consistent. In case that a pixel is only temporally unstable, it is expected that the effect is averaged out. In addition, the problem with inhomogeneous scenes is significantly reduced by this averaging procedure. In case that this analysis is resulting in the detection of possibly unstable pixels, the screening and calibration subsystems are informed.

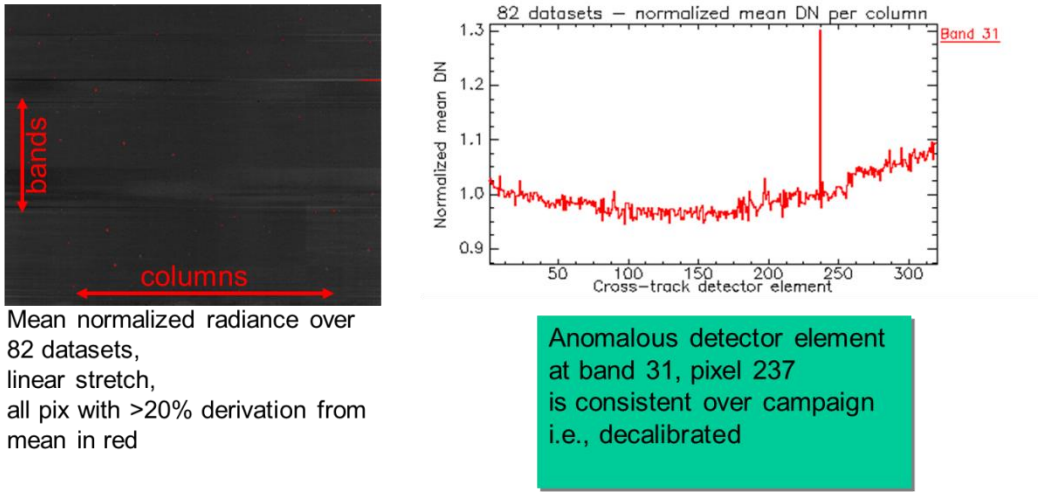

Figure 6-5 Example for analysing multiple HySpex detector maps.

3) Analysis for banding:

Affected band over all columns has higher or lower radiance and low correlation with adjacent bands

$$L_{DM}(k) - 0.5 * (L_{DM}(k+1) + L_{DM}(k-1)) > threshold$$

$$r(L_{DM}(k), L_{DM}(k+1)) < threshold \quad \text{AND} \quad r(L_{DM}(k), L_{DM}(k-1)) < threshold$$

using the thresholds of DN=200.

Note that the analysis must consider also additional influencing factors like bands within atmospheric absorptions, or where dominant materials have narrow absorption features. Automated tests can be carried out for these suitable bands.

6.4.4 Analysis for spectral smile indication

For the detection of spectral smile using image data, narrow atmospheric absorption bands like the 0_2 absorption at 760 nm are frequently used (see Fig. 6-6).

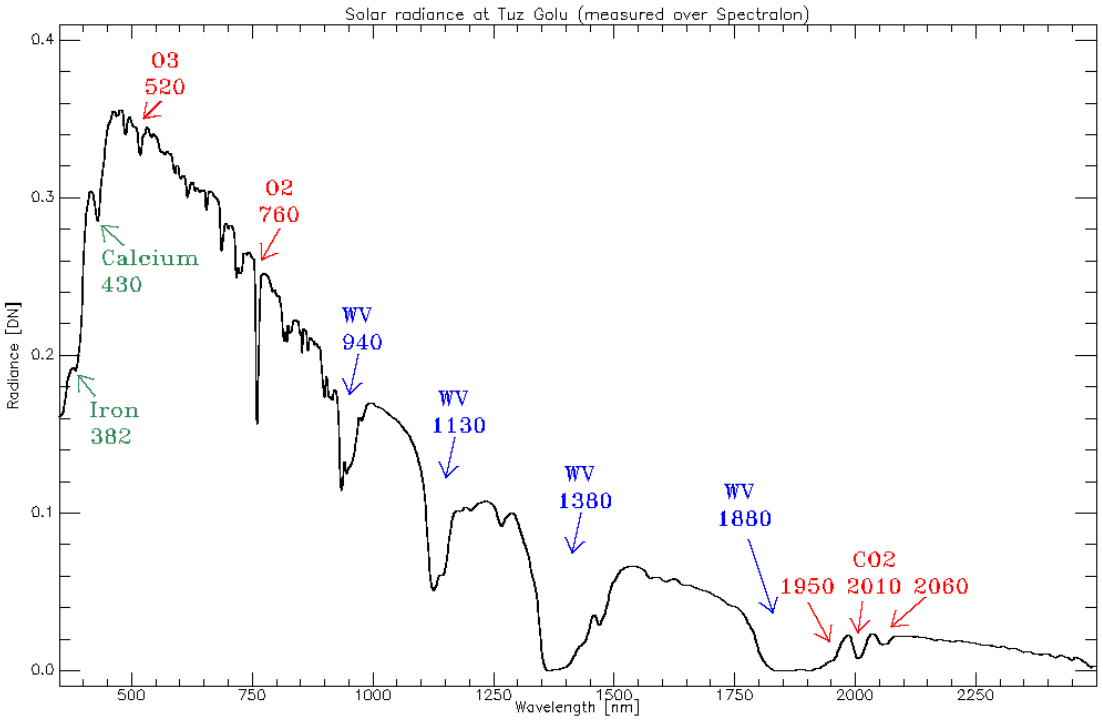

Figure 6-6 Example for a radiance spectrum measured with ~ 3nm bandwidth from 350-1000nm and ~10nm for wavelength >1000nm; Fraunhofer lines in green, Water Vapor absorptions in blue, gas absorptions in red. Note that DN values are given for the radiance because of a known de-calibration of the measurements.

An automated approach related to the spectral data properties is based on the radiance detector maps. As shown in Figure 6-7 below, the detector maps show a brightness gradient in cross-track scanning direction for bands at the edges of narrow-band atmospheric absorption features (in the illustration, HySpex SWIR band 173). Even though this indication is not as precise as other approaches, the benefit of the usage of the detector maps is that datasets can be analysed automatically.

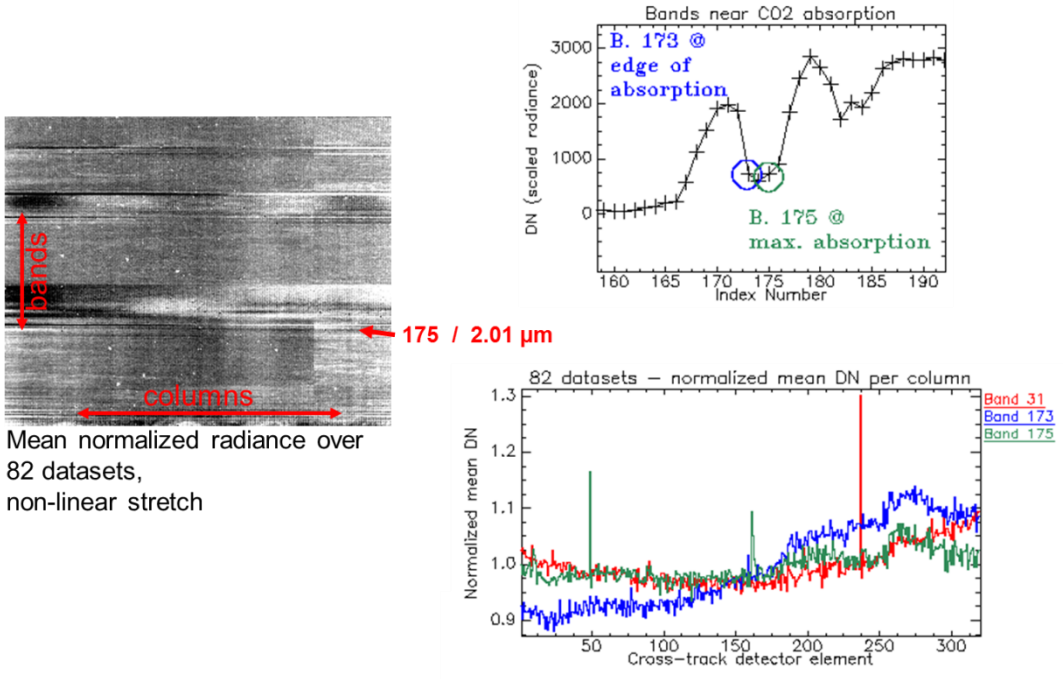

Figure 6-7 Illustration for the detection of uncorrected spectral smile using the Detector Maps of 82 airbrone HySpex datasets. Note that the SWIR wavelength region is depicted in this example, but the same principle is valid also for the VNIR wavelength region using different atmospheric absorption bands (see Fig. 6-6).

For this purpose, the cross-track profile is calculated for bands at the steep edges of atmospheric absorption bands (e.g., band 173 in the example above). Subsequently cross-track profiles for bands without any narrow absorption bands but in neighbouring wavelength regions are also calculated (e.g., band 175 in the example above). Finally an indication for spectral smile can be derived if the absolute difference between smile-affected cross-track profiles and non-smile affected cross-track profiles exceeds a certain threshold of DN=100000, i.e.

$$abs(\, L_{DM}\,(k_{nosmile}) - L_{DM}\,(k_{smile})) < threshold$$

6.5 Spectral Referencing

For spectral referencing, the L1B Processor uses Spectral calibration data (from Spectral Calibration Data Package)., which are provided by the on-board spectral calibration measurements.

Each band gets assigned wavelength information. Spectral referencing of each pixel to its spectral response function is described by a centre wavelength and FWHM which are both stored in the spectral calibration table [AD04] and are a part of a Spectral Calibration Data Package. While monitoring and possible updating of the central wavelength is part of the on-board calibration concept, the FWHM is not examined with the on-board calibration unit (LEDs). The FWHM is only measured pre-launch in the laboratory and is included in the spectral calibration table as a fixed parameter set.

6.6 Abnormal Pixel Interpolation

As described in 6.4, the quality analyses identify precisely the pixels with an abnormal behaviour. Before continuing the systematic corrections an interpolation of these flagged pixels is performed. This interpolation aims to minimize the impact of the abnormal pixels in the final processing steps of the L1B

processor which also perform several interpolation procedures over the image in order to correct systematic effects like rolling shutter (6.7), smile (6.8.1), and keystone (6.8.2). The hybrid interpolation method for abnormal pixels selects the optimum value between spectral and spatial cubic spline interpolation. The selection criterion is based on the spectral gradient difference between the interpolated pixels and spatial neighbours.

6.7 Rolling Shutter

The DESIS sensor has a CMOS detector and a configurable rolling or global shutter mode. The rolling shutter mode enables higher frame rate and better SNR than global shutter. The drawback of the rolling shutter is that each scan line (row) of a sensor is collected at a different time. The baseline for Earth DT and corresponding Dark Current and Calibration data takes is a rolling shutter mode configuration.

Rolling shutter causes that every scan line (row, channel) of a frame is collected at a (slightly) different time. The exposure of a scan line (row) k in a frame i begings after the end of the exposure and readout of this scan line k in a frame $i-1$. Thus, each channel in a frame measures reflections from a different area on the ground due to the time delay δt between the beginnings of exposures between scan lines. See [AD11] for details. The exposure time of each scan line is constant.

A frame rate is determined by the exposure and read out time. Before the exposure the values in the scan line have to be reset or initialized. Even if scan lines in a frame are collected with a time delay, the acquisition time of a frame is always referred to as an acquisition time of the certain spectral channel in the frame. The number of this spectral channel is defined in 5.2 Raw Data and Virtual Channel. The L1B processor accounts for the shift between scan lines in a frame.

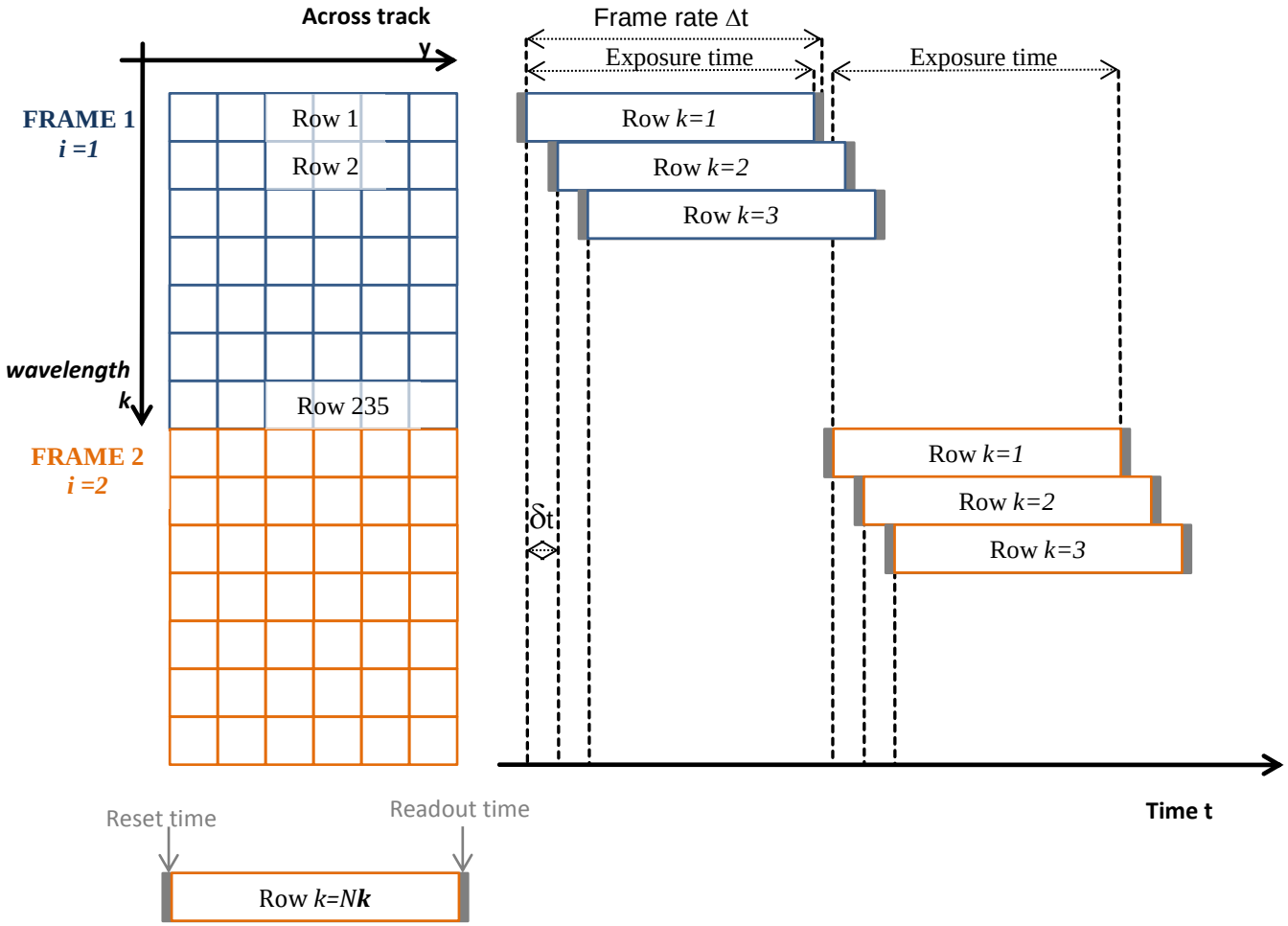

Figure 6-8 Rolling shutter and time delay of exposure of subsequent scan lines (rows) in one frame.

6.8 Smile and Keystone Correction

The spectral smile and keystone effects are inherent to every pushbroom sensor. While spectral smile results on a variation of the channel central wavelength, keystone introduces a spatial misregistration. Figure 6-8a shows the ideal sensor geometry of every frame while Figure 6-8b represents the distorted geometry of the real sensor due to the mentioned effects. The Smile and keystone effect corrections aim to correct the real geometry to the ideal.

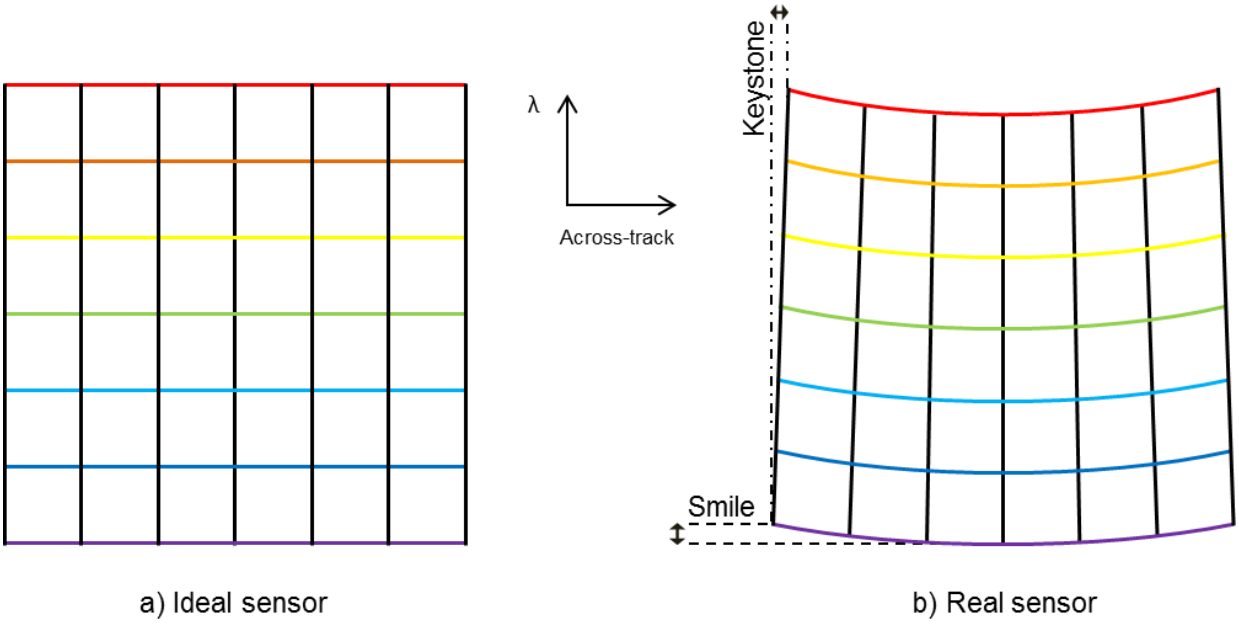

Figure 6-9 Influence of Smile and Keystone effects on the sensor geometry.

6.8.1 Smile Correction

Taking the measured central wavelength on the sensor's centre as the nominal central wavelength, the spectral smile produces a shift on the measured central wavelength with maximum values at the sensor edges.in the across track direction. The smile correction is performed using bi-cubic interpolation over the obtained data which is referenced using the applicable Spectral calibration data.

6.8.2 Keystone Correction

No keystone correction necessary, because this effect is far below on pixel

6.9 Radiometric Referencing

All systematic and radiometric calculations are performed in float numbers thus resulting in radiance values stored in variable L. For storage saving purposes, the L1B product is defined as integer type. To use the whole range of integer representation, the float (32 bit) to unsigned integer (16 bit) transformation is implemented by

$$L_{i,j,k}^{\text{int}} = \text{int}\left(\frac{L_{i,j,k} - O_k}{F_k}\right) \quad (6\text{-}6)$$

where

$L_{i,j,k}^{int}$ is the integer 16 bit representation of the radiances of the whole Earth data take,

$L_{i,j,k}$ is the radiance representation of the entire Earth data take,

and radiometric referencing factor (F) and radiometric offset (O) for absolute radiometric referencing are defined per channel k as

$$F_k = \frac{\max(L_{i,j,k}) - \min(L_{i,j,k})}{2^{16} - 1} \quad (6\text{-}7)$$

$$O_k = \min(L_{i,j,k}) \quad (6\text{-}8)$$

F_k and O_k are both stored in the L1B product metadata. In this way, users could perform a backward transformation from integer representation to physically meaningful radiance values by

$$L_{i,j,k} = L_{i,j,k}^{\text{int}} \cdot F_k + O_k \quad (6\text{-}9)$$

The final Level 1B Data Product is a hyperspectral cube (3D array) containing digital numbers $L_{i,j,k}^{int}$ free of systematic and radiometric errors. Moreover, the resulting product bands are characterised spectrally by a central wavelength, and FWHM; and radiometrically by a factor F and an offset O. These characterisations allow the user to convert the digital integer numbers to absolute radiances.

6.10 Output Specification

The L1B Processor produces L1B Product, which includes orthorectified DESIS Earth data take tile and quality quicklook file. The L1C Product is prepared for the user delivery. The rolling shutter effect is corrected in L1C Processor.

7. Geometric Correction Processor L1C

Development Level 1C Processor carries out geometric correction of the L1B Earth Products, which accounts for sensor, satellite motion and terrain related geometric distortions. The L1C Product is a geometric corrected image, resampled and transformed to a map projection system.

The process of converting the imagery into map-accurate forms is called orhtorectification. It consists of four main steps:

- Physical model employing Direct Georeferencing (DG), which describes the DESIS instrument. In the following section the scientific background of the physical sensor model as used in DG techniques is described followed by considerations and adjustments for the DESIS sensor model.
- The DEM Intersection model.
- Map projection model.

Notation: Lower indices of vectors (bold lower case letters $\mathbf{r}_{location}^{coordinateFrame}$) denote a location or position and upper indices denote the coordinate frame in which the vector is expressed; lower indices of transformation matrices (bold capital letters $\mathbf{R}_{sourceFrame}^{destinationFrame}$) denote the source and upper indices the destination coordinate frame. Scalars are denoted by lower case letters.

7.1 Input

Input data	Output data	Auxiliary data • Before Launch	 After Launch
• L1B Product (one tile)	• L1C Product	• Global DEM database • Global Reference database • Geometric calibration tables	• No update • STS/gyros measurements • Update part of the tables

Table 7-1 Parameters for Geometric Correction Processor L1C

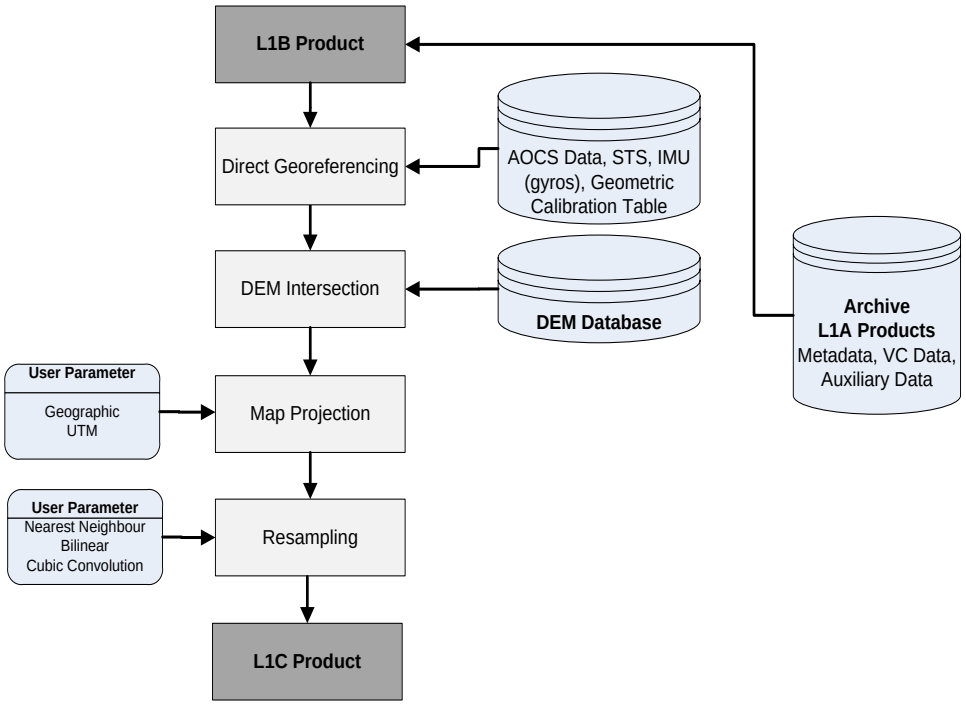

Figure 7-1 Overview of the Systematic and Radiometric Correction Processor L1B.

7.2 DESIS/MUSES Coordinate Frames

The following coordinate frames have to be considered in the L1C Processor:

- The position and velocity (State vector) of the ISS is measured in Earth Centered Rotational (ECR, also named Earth Centered, Earth-Fixed ECEF) frame and is transmitted to the MUSES platform within the Broadcast Ancillary Data (BAD)..
- Mount (body, STS) frame is fixed to the MUSES platform. The platform has two gimbals. The inner gimbal rotates the platform around x-axis in (predominantly along-track direction). The outer gimbal rotates the platform around y-axis in (predominantly across-track direction). A STS and gyros are rigidly mounted on the MUSES platform and provide measurements of the attitude angles w.r.t. an inertial frame (ECI) transformed to ECR angles on ground. .
- Sensor (cube) frame is fixed to the DESIS instrument. The DESIS is mounted in one of the four slots of the MUSES platform. Pointing of the sensor is achieved through the POI. POI allows for tilting±15° in predominantly along track direction, which corresponds to the mirror movement of ±7.5°.
- Focal plan coordinate frame is fixed on the CMOS sensor of the DESIS. The mapping of the pixel location to the sensor frame is defined through geometrical calibration (laboratory measurement and in flight calibration).

7.3 Direct Georeferencing and Line-of-Sight Model

The Direct Georeferencing is based on the Line-of-Sight (LoS) model for each pixel. LoS model analytically describes projection of every pixel in focal plane onto the surface of the earth in terms of earth bounded coordinate frames. It utilizes on board measurements from STS, gyros, GNSS (for determination of exterior orientation), and laboratory and/or in-flight geometric characterisation of the sensor (for determination of interior orientation). The pixel LoS vector is time dependant.

The functional model for Direct Georeferencing is based on the collinearity equation and relates the measured pixel location $\mathbf{r}_{object}^{sensor}$ in the focal plane, expressed in the sensor coordinate frame, to the corresponding object location $\mathbf{r}_{object}^{earth}$ of the light reflecting target, expressed in an earth bound coordinate frame. For pushbroom sensors (like DESIS) the law of central projection holds for each scan line acquisition and by consecutive recording of scan lines the image is formed. Let t be the acquisition time of a frame, then the geometric relation between the coordinates of a pixel and the corresponding object point is given by $\mathbf{r}_{object}^{earth}(t) = \mathbf{r}_{sensor}^{earth}(t) + s \cdot \mathbf{R}_{body}^{earth}(t) \cdot \mathbf{R}_{sensor}^{body} \cdot \mathbf{r}_{object}^{sensor}$. Following chapters describe in details each of the processing steps (see Figure 7-2).

$$\mathbf{r}_{object}^{earth}(t) = \mathbf{r}_{sensor}^{earth}(t) + s \cdot \mathbf{R}_{body}^{earth}(t) \cdot \mathbf{R}_{sensor}^{body} \cdot \mathbf{r}_{object}^{sensor}$$

GPS ISS
GPS DESIS

DEM
intersection
model

$\mathbf{R}_{body}^{m}$

Figure 7-2 Direct Georeferencing (basic relation)

7.3.1 DESIS Interior Orientation

The DESIS instrument is geometrically calibrated pre-launch in laboratory. For selected pixels in each wavelength (channel) two object sided pixel view angles ϕ_x (along track) and ϕ_y (across track) are determined. The pixel view angles describe geometric characteristics of the optical system (e.g. lens, mirror, slit distortions) and the sensor detector (e.g. rotation and bending of pixel array). Employing second order polynomial approximation for each pixel in each spectral channel the normalized pixel view vector $\mathbf{r}'^{sensor}_{object}$ can be derived as

$$\mathbf{r}'^{sensor}_{object} = \frac{1}{\sqrt{\tan^2\phi_x + \tan^2\phi_y + 1}} \begin{pmatrix} \tan\phi_x \\ \tan\phi_y \\ -1 \end{pmatrix} \quad (7\text{-}1)$$

```
<interiorOrientation>
        <interiorOrientation>
        <band>
            <bandNumber>0</bandNumber>
            <calAngles>
                <pixelNumber>0</pixelNumber>
                <phiX>0.004739</phiX>
                <phiY>-2.193177</phiY>
            </calAngles>
            <calAngles>
                <pixelNumber>100</pixelNumber>
                <phiX>0.002725</phiX>
                <phiY>-1.762963</phiY>
            </calAngles>
            ….
        </band>
        ….
</interiorOrientation>
```

The interior orientation is given for each band at some selected supporting points in across direction. In order to get the interior orientation at each across track pixel a second order polynomial is estimated. Band number 0 denotes the mean value of all bands.

7.3.2 DESIS Instrument Mounting Angles (Boresight Alignment)

A pointing mirror (POI) allows tilting up to ±15° in along track direction (mirror rotation between -7.5° to +7.5°). Due to uncertainties in commanding the mirror the rotation is extended form -8.5° to +8.5°. The setup is shown Figure 7-3

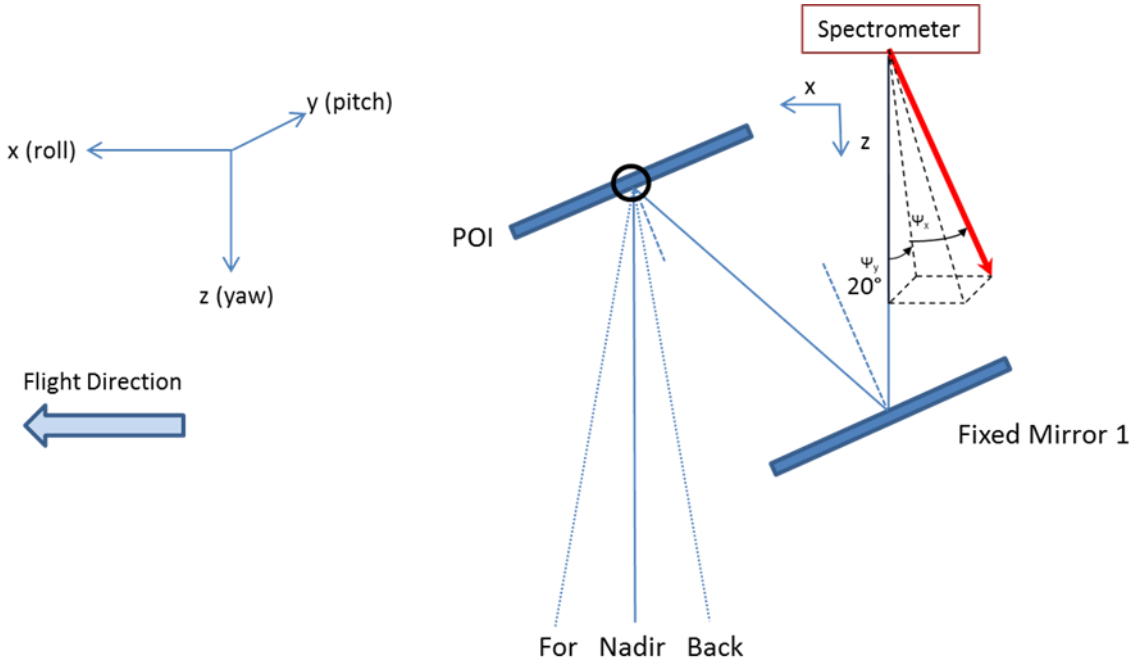

Figure 7-3 Schematic diagram of the POI

The geometric laboratory calibration measurements are performed in the so called FM-O configuration with assembled FPA and ICU components (spectrometer), but without the mirrors (fixed mirror #1 and POI).

We want to derive the Line-of-Sight vectors for each pixel at the POI. The sensor frame, established during the geometric calibration, serves as basic coordinate frame. The normal vectors $(0,0,1)^T$ given in the local coordinate frames of the fixed mirror FM #1 and the POI mirror are coordinated in the sensor frame by

$$n_{FM} = R_x(\Delta\omega_{FM}) \cdot R_z(\Delta\varphi_{FM}) \cdot R_y(\beta_{FM}) \begin{pmatrix} 0 \\ 0 \\ 1 \end{pmatrix}$$

$$n_{POI} = R_x(\Delta\omega_{POI}) \cdot R_z(\Delta\varphi_{POI}) \cdot R_y(\beta_{POI} + \alpha) \begin{pmatrix} 0 \\ 0 \\ 1 \end{pmatrix}$$

The mounting angles of the mirrors have to be calibrated in laboratory (e.g. using alignment cubes). It is noted that the sequence of rotations has to be defined according to the laboratory measurement setup. It is also noted that the sequence of the rotations around the x-axis and the z-axis is not important and can be calculated in small angle representation. The design values are given in Table 7-2

Table 7-2 Design values of mirror mounting angles

Mounting Angle	Design values	Metadata Name
$\Delta\omega_{FM}$	0°	deltaOmegaFM

$\Delta\varphi_{FM}$	0°	deltaPhiFM
β_{FM}	-160°	betaFM
$\Delta\omega_{POI}$	0°	deltaOmegaPOI
$\Delta\varphi_{POI}$	0°	deltaPhiPOI
β_{POI}	20°	betaPOI

Applying the law of reflection for the FM #1 mirror leads to

$$v = r'^{sensor}_{object} - 2 \cdot \left(r'^{sensor}_{object} \cdot n_{FM}\right) \cdot n_{FM}$$

and finally for the POI mirror leads to

$$r^{sensor}_{object} = v - 2 \cdot \left(v \cdot n_{POI}(\alpha)\right) \cdot n_{POI}(\alpha)$$

The POI angles $\{\alpha: -7.5° \leq \alpha \leq +7.5°\}$ are encoded in the POI step given in the session headers of the datatake file and the encoder steps given in the virtual channel of each frame (to be determined by building the mean value of the measurements in the VC for a scene)

Table 7-3 Relation between POI step and POI angle (preliminary settings)

Name	Angle (LOS) [°]	Steps [#]	Angle Encoder Value [#]
Backward	-7.5°	12831	63194276
	-5°	13620	63651648
	-2.5°	14410	64109021
Nadir	0	15200	64566394
	+2.5°	15989	65023767
	+5°	16779	65481140
Forward	+7.5°	17568	65938513

The conversion from POI step to POI angle is therefore given by the linear relationship (note: design values)

$$\alpha = 0.00316627455 \left[\frac{degree}{step}\right] \cdot s - 48.126\ [degree]$$

From the Angle Encoder we get the following relation

$$\alpha = 5.466 \cdot 10^{-6} \left[\frac{degree}{encoder\ step}\right] \cdot e - 352.9199\ [degree]$$

The transformation from the cube coordinate frame to the body (STS) coordinate frame is given by

$$\mathbf{R}^{body}_{sensor} \cdot \mathbf{r}^{sensor}_{object} = \mathbf{R}_{\mathbf{z}}(\theta_z)\mathbf{R}_{\mathbf{x}}(\theta_x)\mathbf{R}_{\mathbf{y}}(\theta_y) \cdot \mathbf{r}^{sensor}_{object} \qquad (7\text{-}2)$$

where the rotation angles are calibrated pre-flight and refined by in-flight calibration procedures.

```
<pointingMirrorAngle>0.0</pointingMirrorAngle>
<deltaOmegaFM>0.0</deltaOmegaFM>
<deltaPhiFM>0.0</deltaPhiFM>
<betaFM>-160</betaFM>
<deltaOmegaPOI>0.0</deltaOmegaPOI>
<deltaPhiPOI>0.0</deltaPhiPOI>
<betaPOI>20</betaPOI>
<boresightAngles>
        <RotX>0.02001</RotX>
        <RotY>0.01004</RotY>
        <RotZ>0.30322</RotZ>
</boresightAngles>
```

7.3.3 Atmospheric Refraction Correction

An atmospheric refraction correction is performed on the view direction vectors of each pixel. Let $\mathbf{r}_{object}^{body} = (x, y, z)^T = \mathbf{R}_{Sensor}^{body} \cdot \mathbf{r}_{object}^{sensor}$ the look direction vector expressed in the body coordinate frame then the atmospheric corrected view direction is

$$\begin{pmatrix} x' \\ y' \\ z' \end{pmatrix}_{object}^{body} = \frac{1}{\sqrt{\delta \cdot x^2 + \delta \cdot y^2 + z^2}} \begin{pmatrix} \delta \cdot x^2 \\ \delta \cdot y^2 \\ z^2 \end{pmatrix} \quad (7\text{-}3)$$

with $\delta = \frac{\tan(\theta - \Delta\theta)}{\tan(\theta)}$

$$\theta = \arctan\left(\frac{x^2 + y^2}{z}\right); \quad \Delta\theta = 2.316 \cdot \tan(\theta) \cdot \left(\frac{P_1 - P_2}{H} - 43.11 \cdot \frac{P_2}{T}\right) + \delta_1 + \delta_2$$

$$\delta_1 = \tan(\theta)\frac{2 + 3 \cdot \tan^2(\theta)}{5} \cdot \delta_1', \quad \delta_2 = 0.129 \cdot \tan(\theta)\frac{e_1 - e_2}{H} + 95 \cdot \frac{e_2}{T},$$

where

H is the nominal satellite altitude in mm (=400e+6),

P1 is standard atmospheric pressure at ground in hPa (=1013.25),

P2 is atmospheric pressure at the satellite altitude in hPa (=0),

T is atmospheric temperature at satellite altitude in K (=1000),

δ1′ is earth curvature correction coefficient in radian (=0.812e-6),

e1 is vapour pressure at ground in hPa (=17.06),

e2 is vapour pressure at satellite altitude in hPa (=0).

The magnitude of the ground displacement caused by atmospheric refraction for off nadir view is given in Table 7-4 [RD44].

Off-nadir view [°]	Ground displacement [m]
10	0.5
20	1.2
30	2.2
40	4.0

Table 7-4 The magnitude of the ground displacement caused by atmospheric refraction as a function of off nadir view in space [RD44]

7.3.4 Exterior Orientation

The position and velocity of the ISS is transmitted to the payloads within Broadcast Ancillary Data (BAD). It is assumed that all AOCS data are smoothed and filtered by a Kalman filter. The transformation from the body to the earth fixed coordinate frame is calculated using on-board measurements from the Star Tracker System (+Gyros) and the transformation matrix from the Earth Centred Inertial ECI coordinate frame to the Earth Centred Rotating ECR coordinate frame given by

$$\mathbf{R}_{body}^{m} = R_{ECI}^{ECR} R_{body}^{ECI} \qquad (7\text{-}4)$$

The attitude measurement system outputs unit quaternions $q = (q_1, q_2, q_3, q_4)$ with respect to the ECI coordinate frame (it is noted that the scalar part of the quaternions is given by q1 and the complex part by q2, q3, q4). The orthogonal direction cosine rotation matrix (for a right-handed coordinate frame) can be established by

$$R_{body}^{ECI} = \begin{pmatrix} c_{11} & c_{12} & c_{13} \\ c_{21} & c_{22} & c_{23} \\ c_{31} & c_{32} & c_{33} \end{pmatrix} = \begin{pmatrix} q_0^2 + q_1^2 - q_2^2 - q_3^2 & 2\cdot(q_1q_2 + q_0q_3) & 2\cdot(q_1q_3 - q_0q_2) \\ 2\cdot(q_1q_2 - q_0q_3) & q_0^2 + q_2^2 - q_1^2 - q_3^2 & 2\cdot(q_2q_3 + q_0q_1) \\ 2\cdot(q_1q_3 + q_0q_2) & 2\cdot(q_2q_3 - q_0q_1) & q_0^2 + q_3^2 - q_1^2 - q_2^2 \end{pmatrix} \qquad (7\text{-}5)$$

where Euler angles of a specific rotation sequence can be extracted. Due to the definition of the coordinate frame of the space segment (x: nominal starboard; y: nominal velocity vector; z: nominal zenith) the rotation matrix undergoes a additional rotation of -90° around the z-axis, which leads to x: nominal velocity vector; y: nominal backboard; z: nominal zenith. The Euler angles are checked for possible gimbal locks by a RANSAC outlier procedure (linear model assumed) and corrected by a linear model. For DESIS the sequence pitch-roll-yaw (φ-ω-κ) is used, which leads to the Euler angles

$$\omega = \arcsin(c_{23}) \qquad (7\text{-}6)$$

$$\varphi = \arctan 2\left(-\frac{c_{13}}{c_{33}}\right)$$

$$\kappa = \arctan 2\left(-\frac{c_{21}}{c_{22}}\right)$$

The extracted Euler angles at a scan line time are linearly interpolated. The resulting attitude angles are checked for gimbal locks using RANSAC (random sample consensus) with a linear regression model.

In case the quaternions are given with respect to ECI

If the reference frame (see metadata tag “reference frame”) is ECI the following transformation matrices from ECI (J2000) to ECR (ITRF89) is applied (see [RD48])

$$R_{ECI}^{ECR} = R_{XY} \cdot R_{GAST} \cdot R_{PN} \qquad (7\text{-}7)$$

where

R_{XY} is the polar motion matrix,

R_{PN} is the nutation and precession matrix,

R_{GAST} accounts for the earth rotation using Greenwich Apparent Sidereal Time.

The current information on the Earth’s orientation in the IERS Reference System is downloaded from the server provided by the International Earth Rotation and Reference System Service (http://www.iers.org). This includes Universal Time, coordinates of the terrestrial pole, and celestial pole. The transformations from ECI to ECR are performed using the SOFA (Standards Of Fundamental Astronomy) library functions.

In case the quaternions are given with respect to ECR (baseline)

If the reference frame (see metadata tag "referenceFrame") is ECR then the quaternions reported in the product metadata file are already corrected for any leverarms (related to the platform coordinate frame) and given as angles in the ECR frame.

The position $\mathbf{r}_{sensor}^{earth}$ of the sensor projection centre is given by

$$\mathbf{r}_{sensor}^{earth}(t) = \mathbf{r}_{pos}^{earth}(t) - \mathbf{R}_{body}^{earth}(t) \cdot \mathbf{r}_{pos}^{body} \qquad (7\text{-}8)$$

with $\mathbf{r}_{pos}^{earth}(t)$ the measured position provided by the ISS GPS system within the BAD and $\mathbf{r}_{pos}^{body}$ the lever-arm vector from the origin of the body coordinate frame to the position measurement unit (a constant value during the mission)

```
<attitude>
    <referenceFrame>ECR</referenceFrame>
    <leapSeconds>37</leapSeconds>
    <origin>StarTrackerAndGyro</origin>
    <stateVector>
        <timeUTC>2017-04-15T01:45:12.123456Z</timeUTC>
        <timeGPS>1203223329.123456</timeGPS>
        <angle>
            <q1>-0.2149</q1>
            <q2>0.8186</q2>
            <q3>-0.46456</q3>
            <q4>-0-26042</q4>
        </angle>
    </stateVector>
</attitude>
```

7.3.5 Time Synchronisation and Interpolation

For the DESIS sensor the scan lines are synchronized with the elements of the exterior orientation (state vector and attitude. The ephemeris auxiliary data are calculated for each scan line using Lagrange interpolation. The exact procedure for time synchronisation is described in [AD10]. Let t be the time of the scan line, than the interpolated position $\vec{p}(t)$ and $\vec{v}(t)$ is given by

$$\vec{p}(t) = \sum_{i=1}^{8} \frac{\vec{p}(t_i) \cdot \prod_{j=1, j\neq i}^{8} (t - t_j)}{\prod_{j=1, j\neq i}^{8} (t_i - t_j)} \quad (7\text{-}9)$$

$$\vec{v}(t) = \sum_{i=1}^{8} \frac{\vec{v}(t_i) \cdot \prod_{j=1, j\neq i}^{8} (t - t_j)}{\prod_{j=1, j\neq i}^{8} (t_i - t_j)} \quad (7\text{-}10)$$

using 4 interpolation values of $\vec{p}(t_i)$ and $\vec{v}(t_i)$ before and after time t.

The time t of the scan line is given by

$$t = t_{startTime} + i \cdot \frac{(t_{endTime} - t_{startTime})}{N}$$

```
<temporalCoverage>
    <startTime>2018-02-21T4:42:00.000796<\startTime>
    <endTime>2018-02-21T04:42:05.000141<\endTime>
<\temporalCoverage>
```

with $i = 1, \dots, N$ the line count and N the number of lines in the tile and with $t_{startTime}\ and\ t_{endTime}$ the temporal coverage of the tile (time of first frame / time of last frame) given in the metadata

Note: The GPS time is not disturbed by the leap seconds. To get UTC time use the metadata "leapSeconds" given in the "orbit" and "attitude" section.

The attitude auxiliary data (unit quaternions with 10 Hz repetition rate) are first transformed to Euler angles and then calculated for each scan line using linear interpolation.

```
<orbit>
    <leapSeconds>37</leapSeconds>
    <origin>BAD</origin>
    <stateVector>
        <timeUTC>2018-02-21T04:41:33.099581Z</timeUTC>
        <timeGPS>1203223329.099581</timeGPS>
        <point>
            <location>
                <X>-1201963.28072</X>
                <Y>4261797.26751</Y>
                <Z>-5141720.37676</Z>
            </location>
            <velocity>
                <X>6218.02850634</X>
                <Y>3608.67861145</Y>
                <Z>1540.35206452</Z>
            </velocity>
        </point>
    </stateVector>
</orbit>
```

7.4 DEM Intersection Model

Geometric distortions caused by the terrain are taken into account using Digital Elevation Model (DEM). For geometric correction the ellipsoidal heights are required. Thus, if needed the geoid heights must be transformed into the ellipsoidal heights. The Global DEM Database is used and the object points are determined in an iterative procedure as described below. The result of the DEM intersection model is a scaling factor S (Figure 7-2).

7.4.1 Global DEM Database

A global digital elevation model (GDEM, Figure 7-4) serves as input for the orthorectification process. The DEM is required in order to perform terrain correction within the orthorectification process.

The GDEM database is derived from The Advanced Spaceborne Thermal Emission and Reflection Radiometer (ASTER) and was developed jointly by the NASA and Japan's Ministry of Economy, Trade, and Industry (METI) [RD45]. The characteristics of the GDEM are given in Table 7-5.

```
<processing>
    <versionDEM>GDEM_01.01</versionDEM>
</processing>
```

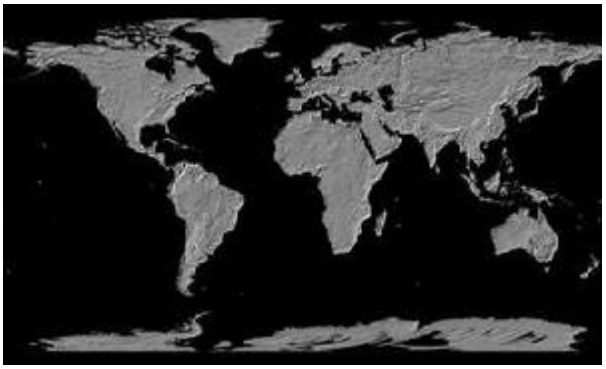

Figure 7-4 Global ASTER DEM [RD45].

Tile Size	3601 x 3601 (1 degree by 1 degree)
Pixel Size	1 arc-second (about 30 m at the equator)
Geographic coordinates	Geographic latitude and longitude
Geoid reference	WGS84/EGM96
Tile volume	North 83 degrees to south 83 degrees, Total: 22 702 tiles
RMSE vertical	Between 10 and 25 m

Table 7-5 GDEM characteristics [RD45].

The geometric displacement Δs caused by the DEM error Δh depends on the off nadir view ω and the terrain slope angle α and is computes as

$$\Delta s = \frac{\Delta h \cdot \tan\omega}{1 - \tan\alpha \cdot \tan\omega} \qquad (7\text{-}11)$$

The geometric displacement for flat and mountainous areas for different off-nadir view angles are given in Table 7-6.

Off-nadir view [°]	Flat area [m] $\Delta h = 6m, \alpha = 0^\circ$	Mountainous area [m] $\Delta h = 30m, \alpha = 20^\circ$
0	0.0	0.0
5	0.5	2.7
10	1.1	5.7

Off-nadir view [°]	Flat area [m] $\Delta h = 6m, \alpha = 0^\circ$	Mountainous area [m] $\Delta h = 30m, \alpha = 20^\circ$
20	2.2	12.6
30	3.5	21.9
40	5.0	36.2

Table 7-6 Displacements caused by the DEM error for flat and mountainous area.

7.4.2 Iterative Determination of Object Points

This step of orthorectification describes the intersection of the pixel view vector with the earth surface. For this purpose a model coordinate frame (index m) is introduced realized by a local topocentric system (LTS). To this end the LoS vectors, the state vectors and the DEM are transformed to a LTS with a fundamental point close to the scene centre, which is derived from the scene corner coordinates. The transformation of the DEM to the model coordinate frame includes a bilinear resampling with a pixel spacing of 30m (similar to the DESIS HSI GSD).

The following iterative technique, illustrated in the Figure 7-5, is established to calculate the intersection point:

- A reference surface at height h_0 is given.
- The analytically calculated intersection point of the sensor look direction with this surface leads to the terrain height h_1 , which is given by the DEM.
- At the height h_1 the intersection with the sensor look direction and a plane is calculated again.
- This procedure is iterated until the horizontal changes are less than the threshold of about half a pixel size. The threshold value (default 0.1 pixel) and maximum number of iterations (default 10) are parameters in the processor

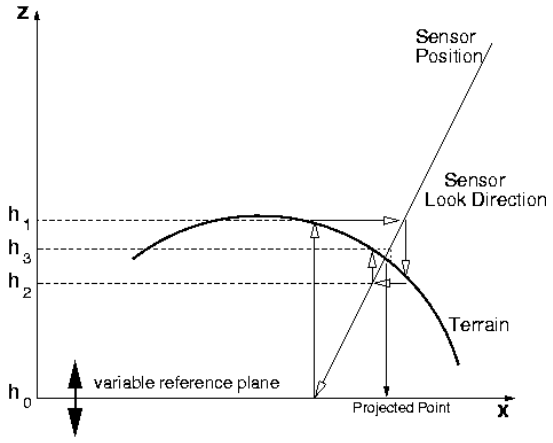

Figure 7-5 Method of determination of the actual sensor look direction with the DEM by an iterative approach.

In order to establish the iterative procedure, first the intersection point with a plane surface at a constant height h_1 with respect to the mapping frame is considered.

Let $\mathbf{r}_{LoS}^{m} = \mathbf{R}_{Sensor}^{m} \cdot \mathbf{r}^{Sensor}$ be the current pixel LoS vector and $\mathbf{r}_{Sensor}^{m}$ the position of the projection centre of the sensor expressed in the mapping frame. The intersection point with a plane surface can be obtained by

$$\mathbf{r}_{Object}^{m} = \mathbf{r}_{Sensor}^{m} + \mu(h_1) \cdot \mathbf{r}_{LoS}^{m} \quad (7\text{-}12)$$

$$\mu(h_1) = \frac{h_1 - (r_z)_{Sensor}^{m}}{(r_z)_{LoS}^{m}} \quad (7\text{-}13)$$

where $(r_z)_{Sensor}^{m}$ and $(r_z)_{LoS}^{m}$ are the z-components of the vectors $\mathbf{r}_{Sensor}^{m}$ and $\mathbf{r}_{LoS}^{m}$ respectively. At the resulting plane co-ordinates of $(r_x)_{Object}^{m}$ and $(r_y)_{Object}^{m}$ the terrain height, given by the DEM expressed in the mapping coordinate frame, defines the new height h_2 of the plane surface, which serves as input for (7-13). Therefore the iteration can be written

$$\mathbf{r}_{Object}^{m}(h_{i+1}) = \mathbf{r}_{Sensor}^{m} + \mu(h_i) \cdot \mathbf{r}_{LoS}^{m} \quad (7\text{-}14)$$

with h_i the terrain height value of the DEM at the plane coordinates of $\mathbf{r}_{Object}^{m}(h_i)$.

The starting terrain height h_0 (reference surface) has to be chosen as close as possible to the final one. Therefore the iterative procedure starts with the mean height values found for the adjacent pixels (the orthoimage processor uses the mean value of three adjacent pixels, which leads to a mean iteration of about 1.1-1.4 cycles in moderate terrain). The point for the start value at height h_0 is calculated by intersection of the actual look direction with an ellipsoid:

Let $\mathbf{p}_{Object}^{ECR} = \mathbf{R}_{Sensor}^{ECR} \cdot \mathbf{r}_{Object}^{Sensor}$ the actual look direction of the sensor and $\mathbf{r}_{Sensor}^{ECR}$ the position of the projection centre of the sensor expressed in the ECR frame, then the intersection point with an ellipsoid can be written to

$$\mathbf{r}_{Object}^{ECR} = \mathbf{r}_{Sensor}^{ECR} + \mu(h_0) \cdot \mathbf{p}_{Object}^{ECR} \quad (7\text{-}15)$$

This intersection point has to fulfil the ellipsoid equation, where $A = a + h_0$ and $B = b + h_0$ with a the major axis, b the minor axis and h_0 the constant height above the earth ellipsoid

$$\frac{(r_x)_{Object}^{ECR\ 2} + (r_y)_{Object}^{ECR\ 2}}{A^2} + \frac{(r_z)_{Object}^{ECR\ 2}}{B^2} = 1 \quad (7\text{-}16)$$

Substituting the components of the vector (7-15) and (7-16) leads to the quadratic equation for the scale factor $\mu(h_0)$

$$\left(\frac{x^2+y^2}{A^2}+\frac{z^2}{B^2}\right)\cdot\mu(h_0)^2+2\cdot\left(\frac{x\cdot x'+y\cdot y'}{A^2}+\frac{z\cdot z'}{B^2}\right)\cdot\mu(h_0)+\left(\frac{x'^2+y'^2}{A^2}+\frac{z'^2}{B^2}-1\right)=0 \quad (7\text{-}17)$$

where $\mathbf{r}_{Sensor}^{ECR}=(x',y',z')^T$ and $\mathbf{p}_{Object}^{ECR}=(x,y,z)^T$.

For the two real solutions for $\mu(h_0)$ of this equation the smaller one (the first intersection with the surface) is used to determine the intersection point of the sensor look directions with a constant height above the ellipsoid surface. The found object point $\mathbf{r}_{Object}^{ECR}$ now can be transformed back to the mapping frame.

The resulting factor $\mu(h_1)$ after iteration is equivalent to the scaling factor s (see Figure 7-2).

7.5 Map Projection

The map projections which are offered as a user input [AD04] to the DESIS L1C product are listed in the Table 7-7. The default projection is the Universal Transverse Mercator (UTM) projection with the central meridian (the UTM one number) derived from the scene center coordinates. The formulas for UTM projections can be found in [RD49] and [RD50].

Identifier	Value range	Comment
Map_Projection	UTM_Zone_of_Center, UTM_Zone_of_Center(-1), UTM_Zone_of_Center(+1), Geographic	The resampling grid will be 30 m for all ISS orbit height

Table 7-7 Supported map projections (user input).

```
<processing>
    <mapProjection>UTM_Zone_of_Center</mapProjection>
</processing>
```

7.6 Resampling

Within the L1C Processor, three image resampling methods are offered as a user input [AD04], these are nearest neighbour, bilinear interpolation (default) and cubic convolution. The bilinear interpolation and the cubic convolution account of the rolling shutter time delay effect, whereas the nearest neighbour interpolation corrects it only to some extent.

Identifier	Value range	Comment
Image_Resampling	Nearest_Neighbor Bilinear_Interpolation (Default) Cubic_Convolution	Cubic_Convolution resampling will result in reduced atmospheric correction accuracy in case of L2A product generation. Nearest Neighbor resampling corrects for the rolling shutter effect only to some extent. The resampling grid will be 30 m for all ISS orbit heights.

Table 7-8 Supported image resampling methods (user input).

The image resampling is based on transformed polygons (triangles) from the image space to the object space as shown in Figure 7-6. The input image grid is covered by a dense net of triangles which are mapped to the output image grid. The resulting triangles are filled by interpolated pixel values using the different resampling methods. A pixel in the output image is inside the triangle if the centre of the pixel is inside the triangle. The inside test is performed with a scan converting algorithm for each pixel in the framing rectangle.

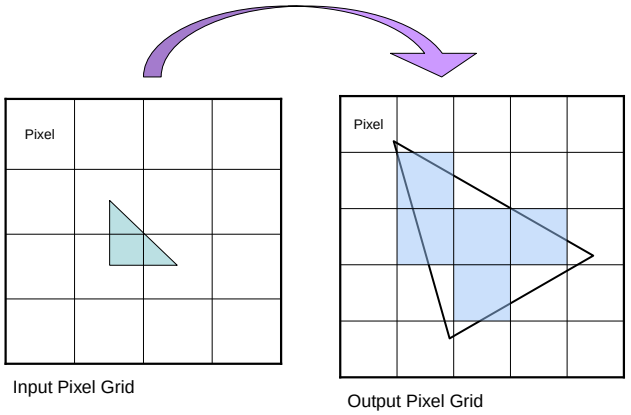

Figure 7-6 Polygons (triangles) of the input image, defined by the centre of adjacent pixels, are transformed to the pixel grid of the orthoimage and filled with bilinear interpolated pixel value

The center of the upper-left corner pixel of the orthorectified scene is a multiple of the image resolution calculated by the formula

$$x_{UL} = x_{\min} - drem(x_{\min}, x_{res}) + \frac{x_{res}}{2} \quad (7\text{-}18)$$

$$y_{UL} = y_{\min} - drem(y_{\min}, y_{res}) - \frac{y_{res}}{2} \quad (7\text{-}19)$$

with the function $drem(a,b) = a - INT(\frac{a}{b})$. The x_{UL}, y_{UL} are the easting and the northing coordinates, respectively.

7.6.1 Nearest Neighbour

Consider a transformed triangle which contains a grid point with the coordinates (x,y) where a new pixel grey value has to be interpolated. Then the grey value at the point (x,y) is given by

$$g(x,y) = g_i(x_i,y_i) \qquad (7\text{-}20)$$

where $i = \min\left\{ i \middle| d_i = \sqrt{(x-x_i)^2 + (y-y_i)^2}; i = 1,\ldots,3 \right\}$.

7.6.2 Bilinear

Consider a transformed triangle, which contains a grid point with the coordinates (x,y). At this point a new pixel grey value has to be interpolated. The grey value at the point (x,y) is then given by

$$g(x,y) = b_1 \cdot x + b_2 \cdot y + b_3 \qquad (7\text{-}21)$$

The three coefficients $\mathbf{b} = (b_1, b_2, b_3)^T$ are determined by the three grey values from the input image at the corner points $g_1(x_1, y_1)$, $g_2(x_2, y_2)$ and $g_3(x_3, y_3)$ of the transformed triangle

$$\begin{pmatrix} b_1 \\ b_2 \\ b_3 \end{pmatrix} = \begin{pmatrix} x_1 & y_1 & 1 \\ x_2 & y_2 & 1 \\ x_3 & y_3 & 1 \end{pmatrix}^{-1} \cdot \begin{pmatrix} g_1 \\ g_2 \\ g_3 \end{pmatrix} \qquad (7\text{-}22)$$

7.6.3 Cubic Convolution

The interpolation at point x can be described by the linear convolution operation

$$g_r(x) = f * g_d = \sum_{i=-\infty}^{\infty} f(x - x_i) \cdot g(x_i) \qquad (7\text{-}23)$$

Where f is the interpolation kernel, $g(x_i)$ is the discrete signal at point x_i, and $g_r(x)$ the interpolated signal at an arbitrary point x. The 4x4 kernel with the free parameter a is given by

$$f(x) = \begin{cases} (a+2) \cdot |x|^3 - (a+3) \cdot x^2 + 1 & |x| \le 1 \\ a \cdot |x|^3 - 5 \cdot a \cdot x^2 + 8 \cdot a \cdot |x| - 4 \cdot a & 1 \le |x| \le 2 \\ 0 & otherwise \end{cases} \qquad (7\text{-}24)$$

For a 2-dimensional grid (equally spaced) the cubic convolution can be separated for the two spatial directions x and y which leads to

$$g_r(x,y) = \begin{pmatrix} f(1+d_y) & f(d_y) & f(1-d_y) & f(2-d_y) \end{pmatrix} \cdot \begin{pmatrix} g(x_1,y_1) & g(x_1,y_2) & g(x_1,y_3) & g(x_1,y_4) \\ g(x_2,y_1) & g(x_2,y_2) & g(x_2,y_3) & g(x_2,y_4) \\ g(x_3,y_1) & g(x_3,y_2) & g(x_3,y_3) & g(x_3,y_4) \\ g(x_4,y_1) & g(x_4,y_2) & g(x_4,y_3) & g(x_4,y_4) \end{pmatrix} \cdot \begin{pmatrix} f(1+d_x) \\ f(d_x) \\ f(1-d_x) \\ f(2-d_x) \end{pmatrix} \quad (7\text{-}25)$$

with $d_x = x - INT(x)$ and $d_y = y - INT(y)$. For the a-factor the value $a = -2/3$ is chosen, which has shown to be optimal for digital images in the sense to approximate the sinc-function.

```
<processing>
        <imageResampling>Bilinear_Interpolation</imageResampling>
</processing>
```

7.7 Sensor Model Improvement

The sensor model improvement is part of geometric calibration. The geometric accuracy of the orthorectified L1C Product is monitored (geometric validation). If the quality is too low, improved sensor parameters (geometric calibration) are computed and provided to the L1C Processor. These improved parameters (calibration tables) are then included in the L1C Processor.

An improvement of sensor model parameters is performed for each image tile on the fly based on automatic generation of Ground Control Points (GCP) using image matching with a reference. These GCPs are used for a least squares adjustment of sensor model parameters (boresight angles). The following steps are performed.

- Geometric affine transformation of DESIS tile based on corner coordinates derived in L1A processing
- Generate mean value of DESIS tile using three channels close to RGB values (depending on binning)
- Apply a WALLIS filter to DESIS tile (window size 21 pixels) => image T
- Resample reference image to resolution of DESIS
- Apply a WALLIS filter to the reference (window size 21 pixels) => image R
- Perform image matching between image T and image R
    - First BRISK (Binary Robust Invariant Scalable Keypoints) matching with outlier detection using affine RANSAC (distance 5 pixels)
    - If BRISK matching fails, perform LLSQ (Local Least Squares) matching with several outlier detection techniques (see [RD51])
    - If LLSQ matching fails, perform SIFT (Scale-Invariant Feature Transform) matching with outlier detection using RANSAC (distance 5 pixels) (see note below)
- Extract best matching points (highest quality figure) based on a 25x25 grid as GCP candidates and separate all other points to a Control Point (ICP) list for quality assessment

- Re-map GCP candidates to image space and complement GCP candidates with terrain heights from interpolated DEM values to get 3D object points
- Estimate improved sensor model parameters for the DESIS tile based on GCP using iterative least squares including outlier removal.

The methodology follows the description given in [RD51] and is not further described here.

Note: State-of-the-Art image matching techniques like BRISK matching [RD52], LLSQ matching [RD51] and SIFT matching [RD53] is used in a cascade.

Note: The SIFT matching is disabled as long as no license is purchased

The quality of geometric correction is given by the RMSE values in meter (degree in case of Geographic mapping) at the ICP in x (east-west) and y (north-south) direction.

```
<orthoRMSE_x>23.97</orthoRMSE_x>
<orthoRMSE_y>21.78</orthoRMSE_y>
<numPointsGCP>462</numPointsGCP>
<numPointsICP>2177</numPointsICP>
<matchingMethod>BRISK</matchingMethod>
```

Note: The accuracy is given w.r.t. the reference image

If no matching can be performed (matchingMethod equals “none”) the calibrated boresight angles are applied, which normally leads to a reduced geometric accuracy.

7.8 Quality Mask Generation

The quality quicklook of L1C data products consists of one file in tif format. This image file contains the same information as for L1B product, but resampled to the new grid resulting from the orthorectification process of the L1C product. The resampling is done by performing first a logical OR operation of the bit pattern of all pixel values involved in the interpolation and filling the mapped triangles (see section 7.6) with these values.

7.9 Output Specification

The L1C Processor produces L1C Product, which includes orthorectified DESIS Earth data take tile and quality quicklook file. The L1C Product is prepared for the user delivery.

8. Atmospheric Correction Processor L2A

This ATBD describes an algorithm for the atmospheric correction of DESIS data over land surfaces using the PACO code (python version of ATCOR code). The method for land is applied over flat or mountainous terrain and converts top-of-atmosphere radiance imagery (L1C) into surface reflectance data (L2A). The flat terrain case is processed with L1C data. In case of a mountainous terrain, a Digital Elevation Model (DEM) is needed to include a correction of topographic effects and the orthorectified (L1C) product is input to the L2A processor.

A DEM processing in L2A is only performed if a corresponding DEM (the DEM has to correspond exactly to the L1C scene and the L1C scene has to be orthorectified using this DEM) is available for the scene and if at least 1% of the scene pixels have slope values greater than a certain threshold (6 degrees).

8.1 Input

The DESIS atmospheric correction processor L2A uses as input the result of the geometric correction processor L1C. The Level 2A product is derived from the Level 1C product, atmospherically corrected and the data converted to ground surface reflectance values.

Input data	Output data	Auxiliary data	
		• Before Launch	After Launch
• L1C Product (one tile)	• L2A Product	• DEM data corresponding to the L1C product	• No update •

Table 8-1 Parameters for Atmospheric Correction Processor L2A

8.2 Algorithm Description

The L2A processor creates a pre-classification map, the aerosol optical thickness map (AOT at 550 nm), columnar water vapour, and the surface reflectance cube, see Figure 8-1.

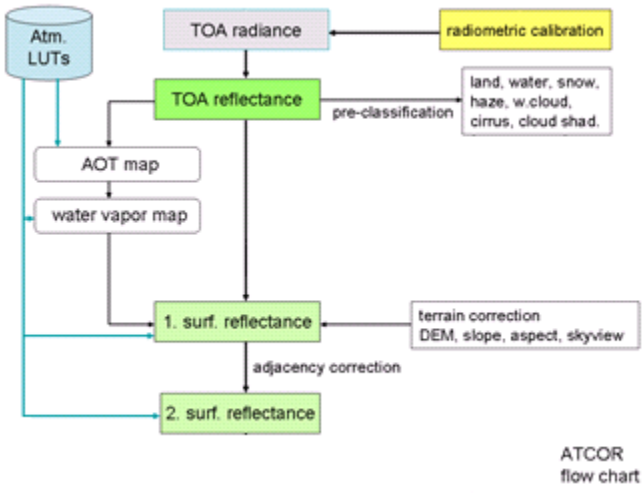

Quality-2

Figure 8-1 Processing of land scenes.

The radiative transfer equation for a homogeneous surface under clear sky conditions is formulated as

$$L = L_p + \frac{\tau \left(E_{dir} \cos\theta_s + E_{dif}\right) \rho / \pi}{1 - \rho\, s} \qquad (8\text{-}1)$$

where L, L_p, τ, E_{dir}, E_{dif}, θ_s, ρ and s are at-sensor radiance, path radiance, ground-to-sensor transmittance, direct and diffuse solar flux on the ground, solar zenith angle, surface reflectance, and spherical albedo of the atmosphere, respectively. The total transmittance is the sum of the direct and diffuse transmittances $\tau = \tau_{dir} + \tau_{dif}$. For brevity, the dependence on wavelength, solar and viewing geometry, and atmospheric parameters has been omitted. A Lambertian or isotropic reflectance law [RD22] is assumed here, as no knowledge of the bidirectional reflectance distribution function (BRDF) is available prior to the atmospheric correction.

For known atmospheric parameters, solar and view geometry, and surface reflectance, the at-sensor or top-of-atmosphere (TOA) radiance is calculated with a radiative transfer code. With remote sensing data from a satellite instrument we have to solve the inverse problem, namely, to derive the atmospheric parameters and surface reflectance from the TOA radiance. A popular approach, also taken for DESIS, is the calculation of a database of look-up tables (LUTs). We use the MODTRAN5.4 radiative transfer code [RD05][RD06] to generate a large database with the required atmospheric functions (path radiance, ground-to-sensor direct and diffuse transmittance, direct and diffuse solar flux, spherical albedo) and a multidimensional linear interpolation is performed to obtain the atmospheric parameters (visibility or aerosol optical thickness at 550 nm and water vapour column).

8.3 Masks for land, water, haze, cloud, shadow

A necessary first step before executing an atmospheric correction is the calculation of a pixel map for haze, cloud, and water. The following table contains the class labels of this map. It shows one class for cloud. The low optical thickness cloud is put into the haze class, which is eliminated. The masks listed in the Table 8-2 are all quality layers of the L2A Data Product [AD04].

Layer	Class
1	Shadow
2	Land (clear)
3	Snow
4	Haze over land
5	Haze over water
6	Cloud over land
7	Cloud over water
8	Water (clear)

Table 8-2 Enhanced classes (land, water, haze, cloud, etc.)

Most of the classes will be defined with spectral criteria, some might need additional information (e.g. “cloud over water” is difficult or impossible to distinguish from “cloud over land” with purely spectral information) which may not be available.

The current algorithm initially assigns the label ‘land’ (clear) to all pixels, reassigning them to other masks along the masking process. During the masking, a pixel will be classified as background if the digital number of any band (up to the red band (around 650 nm)) correspond to the value in the metadata, set in the L1B processor.

The proposed spectral thresholds are empirical and similar to those used in the automated cloud-cover assessment (ACCA) of Landsat ETM+ [RD17] and MODIS [RD04], but experience from the processing of other multispectral sensor imagery (e.g., Ikonos, Sentinel-2, Landsat-8, ALOS-AVNIR2, SPOT-5 etc.) is also being used in defining the thresholds.

This section describes the masking in the ATCOR approach (same as in PACO and, therefore, in L2A processor).

8.3.1 Water class

If the surface elevation of a pixel is lower than 1.2 km above sea level, then the water criterion (blue is 470 nm, green is 550 nm, red is 650 nm, and the NIR is 860 nm band, respectively) is

(8-2)

$$\rho^*_{blue} \leq 0.2 \; and \; \rho^*_{blue} > \rho^*_{green} - 0.03 \; and \; \rho^*_{NIR} < \rho^*_{green}$$

Where the asterisk (*) marks the apparent reflectance.

$$\rho^* = \frac{\pi L}{E_S \cos\theta_S} \qquad (8\text{-}3)$$

where L is the recorded radiance signal, E_s is the extra-terrestrial solar irradiance for the selected band, and θ_s is the solar zenith angle. If the pixel elevation is higher than 1.2 km, the criterion of a negative gradient for the apparent reflectance does not properly work (as the path radiance becomes small) and the following rules with the surface reflectance instead of apparent reflectance are used

$$\rho(NIR) \leq T_{water,NIR} \qquad (8\text{-}4)$$

8.3.2 Cloud over land

Pixels must satisfy the conditions:

$$\rho^*_{blue} > T_c \; and \; \rho^*_{red} > 0.15 \; and \; \rho^*_{NIR}/\rho^*_{red} < 2 \; and \; \rho^*_{NIR} > 0.8\,\rho^*_{red} \; and \; DN_{blue} > T_{saturation}$$

(8-5)

Here, T_c is the cloud threshold as defined in the preference file, default T_c = 0.25.

Note that saturated pixels in visible bands are automatically counted as cloud (if NDSI < 0.7) although they might be something else (e.g., specular reflection from a surface). Other enhanced methods will be tested, e.g. the exploitation of the oxygen feature sensitive to cloud height [RD14]

8.3.3 Snow

Due to the absence of the snow band (SWIR wavelengths) to calculate the ndsi, a set of cuts in the VNIR will be used.

.A relative confusion between clouds and snow pixels might still happen at a certain degree.

This confusion will increase the cloud coverage area with a possible reduction of the products quality.

8.3.4 Shadow

Pixels must satisfy the spectral conditions:

(8-6)

$$\boldsymbol{\rho^*_{red} \leq 0.06 \; and \; \rho^*_{NIR} > \rho^*_{red} + 0.04 \; and \; \rho^*_{NIR} < 0.15}$$

excluding water classified pixels.

Figure 8-2 shows the sequence of masking steps. The map is initialized by assigning all pixels to the land class. Then the cloud, water, and haze classes are assigned.

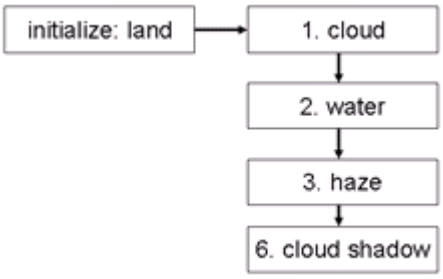

Figure 8-2 Sequence of masking steps before starting the atmospheric correction.

8.4 Radiative transfer calculations and atmospheric database

MODTRAN offers several algorithms for multiple scattering and absorption in the earth's atmosphere: DISORT (discrete-ordinate radiative transfer, [RD38] with and without the azimuth-dependence of the multiple scatter, Isaac's multiple scatter [RD39], and correlated k [RD05] where k indicates the absorption coefficient. The correlated k (CK) approach reformulates the transmittance for a given atmospheric layer as a weighted sum of exponential terms with monochromatic absorption coefficients and probability-depending weighting factors to interface the MODTRAN band model technique with multiple scattering algorithms. After extensive testing, we decided to compile the atmospheric database with the azimuth-dependent scaled DISORT employing 8 streams for the atmospheric window regions [RD15]. The scaled DISORT performs DISORT calculations at 11 fixed wavelengths in window regions and scales Isaac's results to obtain a very fast algorithm. For absorption regions we use the accurate, but time-consuming CK algorithm [RD15]. A straightforward method would use the CK algorithm over the whole spectral range at the highest spectral resolution (1 cm-1). However, this approach is not efficient in terms of computer resources and the referenced paper [RD15] demonstrates that a sufficient accuracy is obtained when employing the CK method to the absorption regions 680 – 840 nm, 890 - 990 nm, 1080 - 1240 nm, 1950 - 2100 nm, and 2300-2500nm. For DESIS sensor only the first two are of interest here.

Calculations were performed for the mid-latitude summer atmosphere (temperature / humidity profile) with a CO2 content of 380 (sea level geometry).

On a global scale, ozone extreme values of 200 – 500 DU can occur, but a more typical range is from 250 - 420 DU. Figure 8-3 shows that relative surface reflectance retrieval errors of up to about 5 - 7 % is expected in the 550 – 600 nm spectrum with the simplification of a constant 330 DU concentration if

compared to concentrations of 250 DU and 410 DU and two reflectance levels (ρ=0.05 and ρ=0.15). All other molecular absorbers in the atmosphere (e.g., O2 , CO, NOx, CH4) are assumed to have constant mixing ratios except for water vapour which varies significantly in space and time.

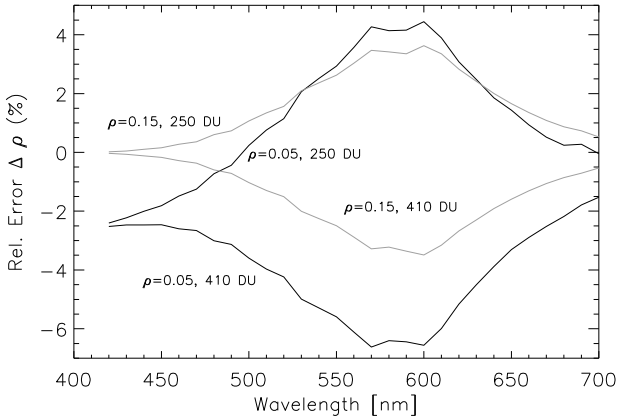

Figure 8-3 Influence of ozone on surface reflectance retrieval.

The ozone information is provided to the DESIS processor (a required user input) and the calibration variables are interpolated given the input ozone value.

No season input is required but it is determine inside the processor using the scene date and the land surface temperature at the scene location from MODIS database MOD11C3.006 [RD54].

The current investigations were performed with the MODTRAN5 code. The original MODTRAN calculations are conducted with a spectrally varying grid (15, 5, and 1 cm-1). In order to expedite later processing steps, all MODTRAN results were resampled to an equidistant 0.6 nm grid using a Gaussian filter curve with FWHM = 0.6 nm, because interpolation on an equidistant grid is much faster than on an arbitrarily spaced grid. This is the final high spectral-resolution (“monochromatic”) database suitable for instruments with bandwidths ≥ 3 nm.

This database is needed for the resampling of the seven atmospheric functions (path radiance, direct and diffuse transmittance ground-to-sensor, direct and diffuse solar flux, spherical albedo and sun-to-ground transmittance) with the channel filter curves. If the spectral calibration changes (central wavelength or FWHM) during the lifetime of a mission, the resampled atmospheric LUTs have to be updated.

Table 8-3 contains the grid points of the atmospheric database in the employed 6-dimensional parameter space (VIS = visibility, SZA = solar zenith angle, RAA = relative azimuth angle between sun and observer line-of-sight, ELE = ground elevation above sea level, TILT=instrument tilt angle, WVC = water vapour column).

Parameter	**#1**	**#2**	**#3**	**#4**	**#5**	**#6**	**#7**	**#8**
VIS (km)	5	7	10	15	23	40	80	120
SZA(deg)	0	10	20	30	40	50	60	70
RAA (deg)	0	30	60	90	120	150	180	
ELE (km)	0	0.7	1.5	2.5	4.0			
TILT (deg)	0	10	20	30	40			

Parameter	#1	#2	#3	#4	#5	#6	#7	#8
WVC (cm) (summer)	0.4	1.0	2.0	2.9	4.0	5.0		
WVC (cm) (winter)	0.2	0.4	0.8	1.1				

Table 8-3 Grid points in the atmospheric database.

The LUT elevation range is 0 – 4.0 km above sea level. Higher elevations are calculated with linear extrapolation of the radiative transfer terms, but elevations > 4 km are treated as a 4 km elevation.

Table 8-3 contains water vapour grid points for the baseline atmosphere (mid-latitude summer) covering the range of 0.4 – 5 cm, values greater than 5 cm will be extrapolated up to 5.5 cm. Water vapour grid points for winter conditions contain a smaller number of grid points because of the smaller dynamic range of 0.2 – 1.1 cm. Values greater than 1.1 cm are extrapolated up to 1.6 cm.

8.5 Extra-terrestrial solar irradiance spectrum

Although the solar constant (wavelength-integrated extra-terrestrial solar irradiance) is known with an accuracy of about 1% there exist large differences between published solar irradiance spectra. Figure 8-4 shows the relative differences between the Kurucz-2005 and the new Kurucz-1997 irradiance spectra in the 0.4 – 2.5 µm spectral region for a Gaussian spectral bandwidth (FWHM = full width at half maximum) of 5 and 10 nm, the typical DESIS range of bandwidths. Similar deviations can also be found with other irradiance spectra.

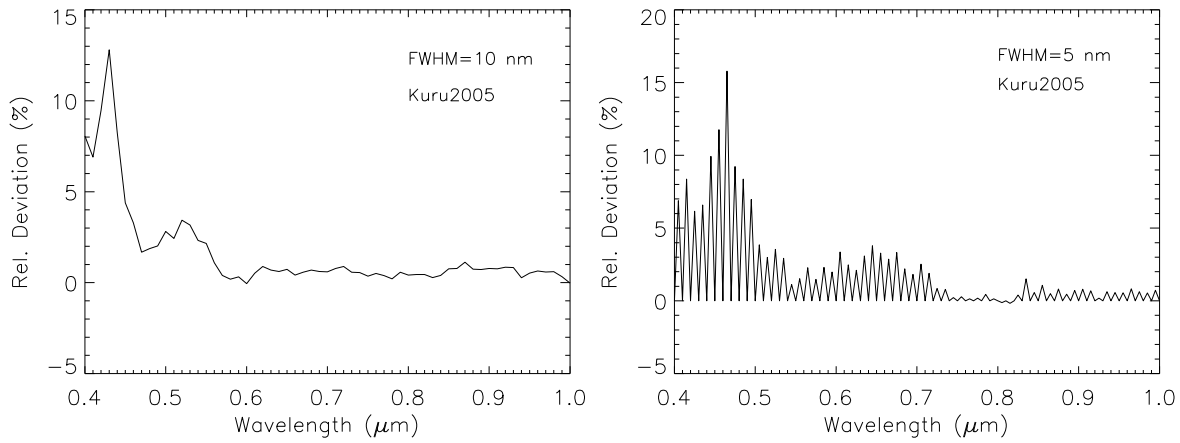

Figure 8-4 Relative deviation (Kurucz2005 – Kurucz1997) / Kurucz1997 .

The atmospheric database for DESIS sensor will be extracted from a monochromatic database LUTs (MODTRAN 5.4.0). Those sensor LUTs (in atm_lib directory) convolve the monochromatic LUTs with an extraterrestrial solar irradiance based on the ‘medium 2’ solar activity of Fontenla (fmed2_2011) [RD55] .

8.6 Retrieval of aerosol optical thickness

Automatic aerosol retrieval over land is performed if the scene contains dark reference areas (dark dense vegetation,) using red and NIR surface reflectance data [RD56]. Then the method can determine the aerosol type and optical thickness.

The NIR and red channels are employed to mask dark pixels in the scene. An atmospheric correction is performed for these channels using the rural aerosol and a visibility of 23 km. With these assumptions, the obtained surface reflectance map is slightly better than with the usual assumption of ρ = ρ* employing the apparent reflectance instead of the surface reflectance. Dark pixels (water) have to be excluded. If more than 2% of the scene pixels are assigned as dark, then the spectral correlation

(8-7)

$$\boldsymbol{\rho_{red} = 0.1\,\rho_{NIR}}$$

is used to estimate the red band (~0.66 µm) surface reflectance for the dark pixels from the NIR reflectance. A consecutive loop over visibility and ρ_{red} improve the estimation of the visibility. In order to cover a large range of aerosols loadings, three visibilities are considered (10, 23 and 60 km) and a mask of dark reference pixels is derived using the ratio vegetation index (RVI) of the red and near-infrared surface reflectance, where RVI=ρ_{NIR}/ρ_{red}, fulfilling the following condition:

$$RVI \geq 3 \; and \; 0.10 \leq \rho_{NIR} \leq 0.25 \; and \; \rho_{red} \leq 0.04$$

The relation $\rho_{blue} = 0.5 * \rho_{red}$ calculates the reflectance in the blue channel (~0.47 µm) from the previously calculated reflectance in the red channel (~0.66 µm). The spectral correlation coefficient (default =0.5) is one of the input parameters specified in the L2A processor default key parameters. The current plan is to apply a fixed correlation coefficient globally due to multiple dependency with other unknown parameters; for example, no seasonal global maps of this coefficient are available for the 30 m spatial resolution of DESIS.

If the reflected signals for the blue and red channels are subtracted from the respective total radiance, the blue/red channel path radiances are obtained. A comparison of L(path, scene, blue) / L(path, scene, red) with the corresponding ratio of MODTRAN aerosols (rural, urban, maritime, desert) can determine the closest MODTRAN aerosol type to our scene. However, for the operational processing we will use the rural (continental) aerosol type and only derive the visibility or aerosol optical thickness (AOT) at 550 nm to avoid possible brightness steps in surface reflectance at tile borders caused by a change in the aerosol type.

Once the surface reflectance ρ(red), ρ(blue) is known for each dark pixel, the at-sensor radiance L(VIS) for the current viewing and solar geometry is calculated as a function of the visibility (or AOT at 550nm) using the pre-calculated LUTs. The intersection of the measured radiance L(measured) with the calculated curve L(VIS) determines the per-pixel visibility which is subsequently smoothed over a 3 km box to reduce noise and decrease the influence of small-scale fluctuations in the spectral correlations (eq. (8-7)).

Additionally, the surface reflectance of water bodies is checked in a red (660 nm) and NIR (850 nm) band. If the selected visibility is too low and causes negative reflectance pixels in the red or NIR bands, it will be iteratively increased up to VIS=80 km. If not enough reference pixels are found, the scene is processed with a constant visibility of 23 km.

It is assumed that the main contribution to the AOT is from aerosols in the lower troposphere (0-2 km boundary layer), small contributions from the upper troposphere (2 – 10 km) and stratosphere are defaulted as per MODTRAN model (e.g. mid-latitude summer).

Details of the aerosol retrieval: after the masking of the reference pixels their surface reflectance in the red channel is calculated with the assumption of a visibility of 23 km. Then eq. (8-7) is employed to calculate the surface reflectance in the blue band, and subsequently the visibility for each reference pixel. In order to remove the influence of instrument noise and variations in the spectral correlation coefficient, a spatial averaging filter (moving window box of 3 km x 3 km) is applied, assigning the average visibility to all gap (i.e., non-reference) pixels. For a faster array addressing the float visibility values (between 5 km and 190

km) are mapped to a discrete integer grid named visibility index (visindex). The visindex=0 corresponds to visibility 190 km, and the visindex increment of 1 corresponds to an AOT increment of 0.006 (at sea level). A second reason for working with the visibility (and corresponding visindex) is that the visibility has only a slight dependence on surface elevation, while AOT varies strongly near steep mountain ridges. Thus, a spatial averaging of visibility/visindex in mountainous regions is not critical. Therefore, the surface reflectance retrieval is performed with the visibility / visindex parameter, and the AOT map is calculated from the visibility map (see eq.(8-8)).

With the MODTRAN code the AOT (at 550nm) is calculated for a given visibility as

$$\mathrm{AOT} = \exp\left\{a(z) + b(z)\,\ln(\mathrm{VIS})\right\} \qquad (8\text{-}8)$$

where z is the surface elevation, and a(z), b(z) are coefficients obtained from a linear regression of ln(AOT) versus ln(VIS).

```
<specific>
        <meanAerosolOpticalThickness>0.2</meanAerosolOpticalThickness>
</specific>
```

8.7 Retrieval of columnar water vapour

The per-pixel columnar water vapour map will be calculated with the APDA (atmospheric pre-corrected differential absorption) algorithm [RD29] using measurement channels around 0.820 µm and appropriate reference or window channels around 0.780 and 0.845 µm, respectively. Since this algorithm is not valid over dark surfaces (water), the water vapour columns over water surfaces will be set to the average value obtained over land.

The basic method uses three channels, one in the atmospheric water vapour absorption region around 940 nm (the "measurement" or “absorption” channel), and the others in the neighbouring window regions ("reference" or “window” channels). The depth of the absorption feature is a measure of the water vapour column content, see Figure 8-5.

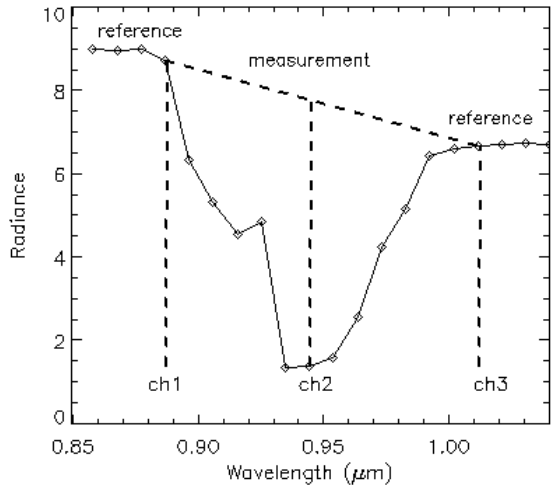

Figure 8-5 Schematic sketch of APDA method with three channels.

For three channels the water vapour dependent APDA ratio is calculated as

$$R_{APDA}(\rho,u) = \frac{L_2(\rho_2) - L_{2,p}}{w_1\left(L_1(\rho_1) - L_{1,p}\right) + w_3\left(L_3(\rho_3) - L_{3,p}\right)} \quad (8\text{-}9)$$

where the index 1 and 3 indicates window channels (e.g., in the 780 – 845 nm region and 1000 nm region), respectively. Index 2 denotes a channel in the absorption region (e.g., 817 - 824nm). L and Lp are the total at-sensor radiance and path radiance, respectively. The symbol u indicates the water vapour column. The weight factors are determined from

$$w_1 = (\lambda_3 - \lambda_2)/(\lambda_3 - \lambda_1) \quad (8\text{-}10)$$
$$w_3 = (\lambda_2 - \lambda_1)/(\lambda_3 - \lambda_1)$$

The problem is the estimation of the surface reflectance ρ_2 in the absorption band. Usually a linear behaviour of surface reflectance is assumed across the absorption region which might influence the water vapour retrieval accuracy if this assumption is violated. The fast and robust APDA method is often used for operational processing [RD35]. Curve-fitting techniques [RD10][RD20][RD21] may achieve a higher accuracy, but are time-consuming and some are not yet operational. Eq. (8-9) is approximated with an exponential fit function using 4 – 6 water vapour grid points for the least squares regression

$$R_{APDA}(u) = exp(-\alpha + \beta\sqrt{u}) \quad (8\text{-}11)$$

which is solved for the water vapour column u :

$$u = \left(\frac{\alpha + ln\, R_{APDA}}{\beta}\right)^2 \quad (8\text{-}12)$$

More than three channels are used with the linear regression ratio (LIRR) method [RD29].

Concerning the selection of channels for water vapour retrieval: it is preferable to employ measurement channels in the 775 – 900nm region to avoid an overlap with the O2 absorption line and spectral absorption features of liquid water in plants.

```
<specific>
        <meanWaterVapour>2.3</meanWaterVapour>
</specific>
```

8.8 Retrieval of surface reflectance in flat terrain

After the aerosol optical thickness and water vapour maps have been calculated, the surface reflectance retrieval is performed. In flat terrain, the radiative transfer equation for a homogeneous surface under clear sky conditions is formulated as:

$$L = L_p + \frac{\tau\left(E_{dir}\cos\theta_s + E_{dif}\right)\rho/\pi}{1 - \rho\, s} \quad (8\text{-}13)$$

where L, Lp, τ, Edir, Edif , θs , ρ and s are at-sensor radiance, path radiance, ground-to-sensor transmittance, direct and diffuse solar flux on the ground, solar zenith angle, surface reflectance, and spherical albedo of the atmosphere, respectively. The total transmittance is the sum of the direct and diffuse transmittances τ = τdir + τdif. For brevity, the dependence on wavelength, solar and viewing geometry, and atmospheric parameters has been omitted.

Eq. (8-13) is solved for the surface reflectance ρ. The initial reflectance image is iterated to take the atmospheric blurring into account ("adjacency effect"). This is caused by photons from the surrounding area that are scattered into the sensor's line-of sight. A simple formulation was proposed by [RD23] where the strength of the adjacency effect is weighted with the ratio q of the diffuse to direct ground-to-sensor transmittance

$$\rho^{(2)}(x,y) = \rho^{(1)}(x,y) + q\left(\rho^{(1)}(x,y) - \overline{\rho}(x,y)\right) \qquad (8\text{-}14)$$

and where ρ(1)(x,y) is the initial surface reflectance image, and $\overline{\rho}$ the ρ(1) reflectance averaged over a square box of size 2 R, where R=1 km is the assumed range of the adjacency effect. The averaging can also be performed with a distance weighting factor [RD25]

$$\rho^{(2)}(x,y) = \rho^{(1)}(x,y) + q\left(\rho^{(1)}(x,y) - \sum_{i=1}^{n} \overline{\rho}_i(x,y)\, w_i\right) \qquad (8\text{-}15)$$

where n is the number of circular rings and wi the exponential distance weighting factor. However, the difference between both approaches is usually small over land areas as the adjacency correction is a second order effect and the spatial pattern of fields tends to repeat itself.

At the scene border the adjacency correction needs information on areas outside the image. Therefore, an estimate is needed, see Figure 8-6. For the original (raw) geometry, a possibility is to mirror the adjacency strip. Another possibility is: if the neighbourhood around a pixel includes a pixel outside the scene the nearest edge pixel is used to compute the box average. The second option is implemented in ATCOR as it is much faster. To reduce the influence of the estimate of the missing area, the weighting factor q in eq. (8-14) is replaced with the factor 0.5 q. In case of a geocoded scene (bottom of Figure 8-6) no adjacency correction is performed in the border strip.

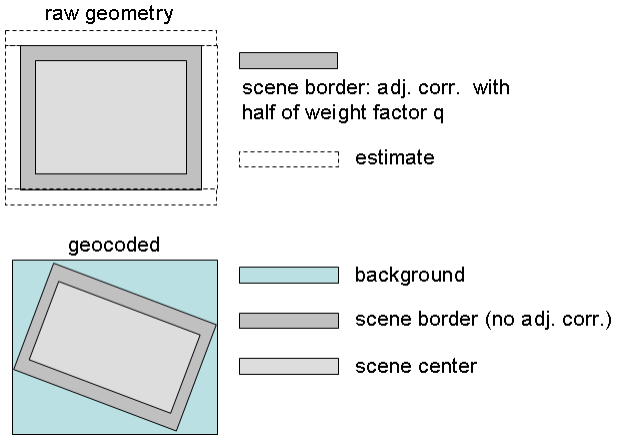

Figure 8-6 Treatment of the adjacency effect.

In the vicinity of clouds a different approach to the adjacency correction has to be taken, because clouds are high in the atmosphere and should not be treated as bright ground surfaces. For the adjacency

correction in equation (8-14) all cloud pixels are assigned the scene average (non-cloud) reflectance $\overline{\rho}$ per channel.

8.9 Retrieval of surface reflectance in mountainous terrain

For each DESIS scene a digital elevation model (DEM) is used. The DEM already has to be matched to the scene, and the derived topographic maps of slope and aspect are calculated in ATCOR. Based on the statistics of the slope map a decision will be made to include a topographic correction as part of the atmospheric correction over land or to process the image assuming a flat terrain with the average elevation according to the DEM. The decision is:

If more than 1% of the scene contains pixels with slopes > 6 degrees, then the topographic correction will be included, otherwise not ("quasi-flat" areas) because artefacts are likely to occur.

In mountainous terrain, the combined atmospheric / topographic correction obviously leads to more complex equations than for the flat terrain case, and some simplifications are applicable. Basically, there are four radiation components contributing to the TOA radiance: path radiance, pixel reflected radiance, adjacency radiation, and reflected radiation from the surrounding topography, see Figure 8-7.

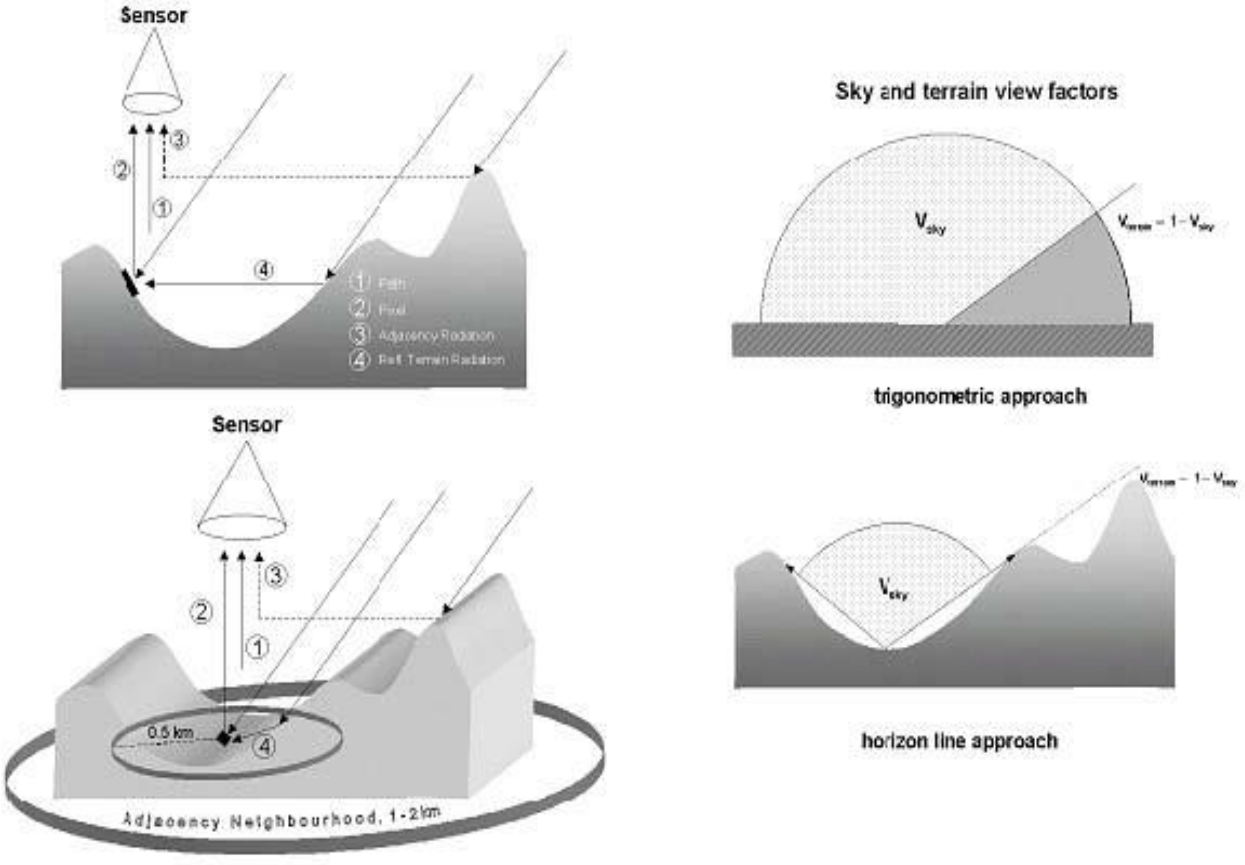

Figure 8-7 Radiation components in mountainous terrain.

The following brief summary follows the paper [RD25]. If $\theta_s, \theta_n, \phi_s, \phi_n$ denote solar zenith angle, terrain slope, solar azimuth and topographic azimuth, respectively, the illumination angle β is obtained from the DEM slope and aspect angles and the solar geometry:

$$cos\,\beta(x,y) = cos\,\theta_s cos\,\theta_n(x,y) + sin\,\theta_s sin\,\theta_n(x,y)\,cos\{\phi_s - \phi_n(x,y)\} \quad (8\text{-}16)$$

The illumination image cos β(x,y) is calculated within ATCOR and stored as separate map. The diffuse solar flux on an inclined plane is calculated with Hay's model ([RD16]):

$$E_d^*(x,y,z) = E_d(z)\left[\, b\,\tau_s(z)\,cos\,\beta(x,y)/cos\,\theta_s + \{1 - b\,\tau_s(z)\}\,V_{sky}(x,y)\,\right] \quad (8\text{-}17)$$

In rugged terrain the radiation reflected from mountains within the line-of-sight of a pixel has to be included as an additional radiance component. The fraction of pixels in the line-of-sight is called terrain view factor (Vt), and it is calculated as

$$V_t = 1 - V_{sky} \quad (8\text{-}18)$$

where Vsky is computed with a ray tracing program [RD09] or as a simple approximation with the local DEM slope value θn :

$$V_{sky} = cos^2(\theta_n / 2) \quad (8\text{-}19)$$

The use of the ray tracing program is recommended for very steep terrain (module skyview of ATCOR creates the corresponding map), in moderately steep terrain the simple approximation is sufficient. It is automatically applied in ATCOR if the "skyview" file name is not specified in the input parameter list or does not exist.

The surface reflectance is calculated iteratively. The first step neglects the adjacency effect and starts with a fixed terrain reflectance of $\overline{\rho}_t^{(0)}$ = 0.1

$$\rho_{(i)}^{(1)}(x,y) = \frac{\pi\left[\, d^2\{c_0 + c_1 DN(x,y)\} - L_p(z,\theta_v,\phi)\,\right]}{\tau_v(z,\theta_v)\left[\, b(x,y)\,E_s\,\tau_s(z)\,cos\,\beta(x,y) + E_{dif}^*(x,y,z) + E_t(z)\,\overline{\rho}_t^{(i)}\,V_t(x,y)\,\right]} \quad (8\text{-}20)$$

The terms are defined as:

x, y horizontal coordinates, corresponding to the georeferenced pixel positions
z vertical coordinate, containing the elevation information from the DEM ;

DN(x,y) digital number of georeferenced pixel ;

$L_p(z,\theta_v,\phi)$ path radiance, dependent on elevation and viewing geometry ;

$\tau_v(z,\theta_v)$ ground-to-sensor view angle transmittance, direct plus diffuse components ;

$\tau_s(z)$ Sun-to-ground beam (direct) transmittance;

$\beta(x,y)$ angle between the solar ray and the surface normal (illumination, eq. (8-16)) ;

b binary factor: b=1 if pixel receives direct solar beam, otherwise b=0 ;

E_s extra-terrestrial solar irradiance (earth-sun distance d=1 astronomical unit);

$E_d^*(x,y,z)$ diffuse solar flux on an inclined plane (see equation (8-17)) ;

$E_g(z)$ global flux (direct plus diffuse flux on a horizontal surf. at elevation z);

$E_t(z)$ terrain radiation reflected from adjacent slopes;

$\overline{\rho}_t^{(0)}$ = 0.1, initial value of average terrain reflectance;

$\overline{\rho}_t^{(i)}(x,y)$ locally varying average terrain reflectance, calculated iteratively;

$V_t(x,y)$ terrain view factor (range 0-1).

The next step iterates eq. (8-20) averaging the reflected radiation over a square box of 0.5 km x 0.5 km. If equation (8-20) is used with $E_t = E_g$ then three iterations are usually sufficient to be independent of the start value of the terrain reflectance [RD25]. However, for highly reflective surfaces (e.g., snow) and high terrain view factors, more than three iterations are necessary and a faster convergence of $\overline{\rho}_t^{(i)}$ is achieved with a geometric series for the terrain reflected radiation E_t as proposed in [RD32]:

$$E_t^{(i)} = E_g \frac{\overline{\rho}_t^{(i-1)}}{1-\overline{\rho}_t^{(i-1)}\overline{V}_t} \qquad (8\text{-}21)$$

The next step is the adjacency correction (eq.(8-14)).

Empirical BRDF correction

For a steep terrain the local solar zenith angle can reach values of 70° to 90° and the Lambertian reflectance assumption causes overcorrected (bright) values. To avoid this behaviour the following empirical approach to topographic correction is taken [RD28]: if the local solar illumination angle β exceeds a threshold βT (i.e., in areas of low illumination where the Lambertian reflectance ρL might become high), the updated surface reflectance is reduced according to:

$$\rho_{MM} = \rho_L \left(\frac{\cos\beta}{\cos\beta_T} \right)^b \qquad (8\text{-}22)$$

The index ‘MM’ stands for modified Minnaert. If the local illumination angle does not exceed the threshold βT, then equation (8-22) is not applied and the Lambertian reflectance is retained (ρMM = ρL). The following set of empirical rules is used:

The threshold angle is set as βT = θs + 25°, i.e., 25° above the solar zenith angle, if θs.< 35°.

If 35°≤ θs ≤ 45° then βT = θs + 20°.

If 45°≤ θs ≤ 50° then βT = θs + 15°.

If 50°≤ θs ≤ 60° then βT = θs + 10°.

If θs > 60° then βT = θs + 10°, i.e., a higher solar zenith angle requires a threshold closer to the solar zenith, because the correction must take place earlier.

Exponent b = 1/2 for non-vegetation

Exponent b = 3/4 for vegetation in the visible spectrum (λ < 720 nm)

Exponent b = 1/3 for vegetation if λ ≥ 720 nm.

In addition, if the correction factor (cosβ /cosβT)b is smaller than 0.25 (i.e., local solar zenith angle much higher than the threshold angle) it will be reset to 0.25 to prevent a too strong reduction. The reference [RD28] demonstrates that this empirical topographic correction approach is usually superior to other commonly employed techniques, but there is currently no method which performs best in all situations.

Figure 8-8 presents an example of a SPOT-5 scene from Switzerland [RD28] with a combined atmospheric and topographic correction including the empirical BRDF correction of eq. (8-22). The left part shows the colour coded scene (RGB = 1650, 840, 660 nm), the central part contains the illumination map, and the right part the surface reflectance product. Most of the topographic features are successfully eliminated.

Figure 8-8 SPOT-5 scene from Switzerland with topographic correction

8.10 Input: Land Surface Temperature (LST) database

For the season selection a MODIS database (monthly during one year) should be provided in the previously described “atm_database” directory with the following structure:
<atm_database_parent_directory>/MODIS/MOLT/<modis_product>/<YYYY.MM.01>/
where <modis_product> is “MOD11C3.006”.
Inside each first day of the month a hierarchical data format file (.hdf) table must exists (e.g. of the file name MOD11C3.A2008001.006.2015338162249.hdf)

8.11 Output files

The L2A Products are prepared for the user delivery:

- Surface reflectance cube (percent reflectance, usually with a scale factor of 100). 16 bit signed integer file, all channels stacked in one file, geotiff format, one file.

- L2A Quality cube from L1C product (orthorectified) containining pixels information from L1B:
    - Layer 1: Quality Layer with the number of "Excluded pixels" in the spectral domain for a given x-y pixel in the spatial domain. Excluded pixels are those that are either "Dead Pixels" or "Abnormal Pixels".
    - Layer 2: Quality Layer with the number of "Too High Radiance pixels" in the spectral domain for a given x-y pixel in the spatial domain.
    - Layer 3: Quality Layer with the number of "Too Low Radiance pixels" in the spectral domain for a given x-y pixel in the spatial domain.
- L2A Quality cube (ten unsigned 8-bit layers of NxM pixels in geotiff format (N and M are the same values as in the L1C data product):
    -
    -
    -
    - Layer 1: Shadow pixel, a 0/1 value for each pixel in the quicklook with spatial "i" and "j" coordinates indicating if the pixel is classified as shadow (1) or not (0).
    - Layer 2: Land pixel (clear), a 0/1 value for each pixel in the quicklook with spatial "i" and "j" coordinates indicating if the pixel is classified as land (1) or not (0).
    - Layer 3: Snow pixel, a 0/1 value for each pixel in the quicklook with spatial "i" and "j" coordinates indicating if the pixel is classified as snow/ice (1) or not (0).
    - Layer 4: Haze over land pixel, a 0/1 value for each pixel in the quicklook with spatial "i" and "j" coordinates indicating if the pixel is classified as haze over land (1) or not (0).
    - Layer 5: Haze over water pixel, a 0/1 value for each pixel in the quicklook with spatial "i" and "j" coordinates indicating if the pixel is classified as haze over water (1) or not (0).
    - Layer 6: Cloud over land pixel, a 0/1 value for each pixel in the quicklook with spatial "i" and "j" coordinates indicating if the pixel is classified as cloud over land (1) or not (0).
    - Layer 7: Cloud over water pixel, a 0/1 value for each pixel in the quicklook with spatial "i" and "j" coordinates indicating if the pixel is classified as cloud over water (1) or not (0).
    - Layer 8: Water pixel (clear), a 0/1 value for each pixel in the quicklook with spatial "i" and "j" coordinates indicating if the pixel is classified as water (1) or not (0).
    - Layer 9: Aerosol optical thickness (at 550 nm), scaling factor100, value encoded in 8-bit unsigned format. Maximum possible OAT value of 2.5.
    - Layer 10: Perceptible water vapour, scaling factor 42, value encoded in 8-bit unsigned format. Maximum possible value of 6.0 cm.
- A file with one 8-bit (unsigned) layer of j x k pixels(cross-track pixels x spectral bands) in geotiff format:
    - Layer 1: Quality layer with the detector map value of cross-track pixel j and band-k at pixel position i-k. The detector map value is encoded in the 8-bit values.

8.12 L2A quality flags

Flag	Comment
Average scene water vapour content	If WV > 4cm: reduced quality, WV > 5cm: low quality
Average scene visibility / aerosol optical thickness	If VIS < 10km: reduced quality, VIS <7km: low quality

Flag	Comment
Low sun angle	If SZA >55: reduced quality, SZA > 65: low quality
Percentage of haze	If percent of haze > 20%: reducedquality
Percentage of clouds	If percent of clouds > 20%: reducedquality
Percentage of cloud shadow	If percent of cloud shadow >10%: reduced quality
Percentage of topographic shadow	If percent of topographic shadows > 10%: reduced quality

Table 8-4 L2A quality flags

Appendix A

8.13 Appendix: Altitude profile of summer and winter atmospheres

The following two tables contain the altitude profiles of the MODTRAN atmospheres mid-latitude summer and mid-latitude winter for the 0 – 5 km height range.

Altitude	pressure	temperature	rel. humidity	abs. humidity
(km)	(mbar)	(°C)	(%)	(g/m3)
0	1013	21.0	76	13.9
1	902	16.5	66	9.3
2	802	12.0	55	5.9
3	710	6.0	45	3.9
4	628	0.0	39	1.9
5	554	-6.0	31	1.0

Table A1.1 Altitude profile of the mid-latitude summer atmosphere.

Total (ground-to-space) water vapour content = 2.92 (cm or g cm-2).

Altitude	pressure	temperature	rel. humidity	abs. humidity
(km)	(mbar)	(°C)	(%)	(g/m3)
0	1017	-1.0	77	3.5
1	897	-4.5	70	2.5
2	789	-8.0	65	1.8
3	694	-11.5	57	1.2
4	608	-17.5	50	0.7
5	531	-23.5	47	0.4

Table A1.2 Altitude profile of the mid-latitude winter atmosphere.

Total (ground-to-space) water vapour content = 0.85 (cm or g cm-2),

A.1 Appendix: Selection of atmospheric LUTs

The high spectral resolution (“monochromatic” *.bp7) LUTs are offline resampled with the DESIS channel filter functions to obtain the DESIS specific LUTs (*.atm). The monochromatic database is calculated off-line, and the resampling has to be conducted only once if the spectral filter functions are stable. If not, the spectral resampling is needed if a change in the filter functions occurs. In this case, a time stamp of the spectral calibration and LUTs is required. The resampled LUTs will be used during atmospheric correction.

A.1.1 Appendix: LUT names

The LUT names include the aerosol type (e.g. rural), water vapour grid (e.g. wv=04 meaning wv=0.4 cm for the sea level) and a summer /winter.

The default ozone DU simulated, changes with the season: 330 DU for summer and 377 DU for winter. To correct for other ozone column values per scene, a set of correction tables are loaded during the processing: “ozone_luts.bin” (for summer) and “ozone_luts_winter.bin” (winter).

The same names are applied for the monochromatic and resampled LUTs, only the file extension is different (.bp7 for monochromatic LUTs, .atm for resampled LUTs).

Summer LUTs

File name

h99000_wvxx_rura

where xx is a two letter water vapour grid identifier: xx = 04, 10, 20, 29, 40, 50

(xx=20 means water vapour column 2.0 cm from sea level to space).

Winter LUTs

File name

w99000_wvxx_rura

9. Open Issues

All open and undecided questions in this document, are marked as To Be Defined (TBD) and are summarized in the following table Most of the TBD will be clarified after the final instrument design is available.

TBD ID Topic	Comment	Expected Resolving
[TBD01] Compression of raw data	No compression of raw data	To be confirmed by TBE Resolved – no compression
[TBD02] Format of tasking and catalogue order data	Format is the same	To be confirmed by TBE Resolved
[TBD03] Number of virtual channels in a frame Rolling shutter and time tagging of frames	2 VC in each Frame are defined One might be sufficient.	To be confirmed by SS DLR/OS Resolved – 2xVC accepted
[TBD04] Monitoring of parameters from a virtual channel	Define parameters from a virtual channel to be monitored.	Input by SS DLR/OS Resolved – Screening parameters defined
[TBD05] Max number of tiles in a data take	The maximum number of tiles in a data take has to be defined	Phase D Resolved – 100 tiles max
[TBD06] Metadata file parameters for tiling of a data take	Parameters of the metadata file: Tile ID, Number of Tiles. Some other might have to be defined.	Phase D Resolved – GUID+TileID = unique tile identifier
[TBD07] A need for Gain Matching table	Current baseline is that no Gain Matching table is used.	To be confirmed SS DLR/OS Resolved
[TBD08] Content and format of the Experimental Data Products	Information about the Experimental data products is needed to decide, if the screening and dark current extraction procedures can be applied.	To be defined by SS Resolved
[TBD09] Saturated Radiance Value	To be adjusted depending on the linearity of the instrument's response.	Input by SS DLR/OS No linearity provided by instrument team - skipped
[TBD10] Low Signal Value	To be adjusted depending on the linearity of the instrument's response.	Input by SS DLR/OS No linearity provided by instrument team - skipped
[TBD11] Alpha value for striping / lining	To be adjusted depending on the instrument actual spatial stability	Commissioning phase E1. Preliminary thresholds provided.
[TBD12] Earth Data Takes acquired in a rolling shutter mode	Confirm if all Earth Data Takes are going to be acquired in a rolling shutter mode	Check with SS, DLR/OS Resolved – RS is baseline, GS is experimental
[TBD13] BAD data in [ft/s]	Are Broadcast Ancillary Data (BAD) in [ft/s]? Then conversion to SI units [m/s] needed.	Check with TBE Resolved
[TBD14] Input AOCS data smoothed and filtered by a Kalman filter	Confirm if AOCS data are smoothed and filtered by a Kalman filter.	Check with TBE Resolved – data coming with 10 Hz smoothed and interpolated

TBD ID Topic	Comment	Expected Resolving
[TBD15] Hz of quaternions	Repetition rate (Hz) of auxiliary data is 10 Hz. The number has to be confirmed.	Check with TBE Resolved – 10 Hz is the baseline
[TBD16] DEM Intersection Model depends on the Pointing Knowledge	The pointing knowledge shall be confirmed with TBE.	Check with TBE Partly Resolved – MUSES pointing knowledge known, but not the over-all DESIS pointing knowledge
[TBD17] Mapping between spectral lines and sampling time	Mapping between spectral lines and sampling time must be added/changed after SS provides procedures for it.	Document will be provided by DD DLR/OS Resolved
[TBD18] Aerosol optical thickness map - output	To deliver the aerosol optical thickness map (forgotten)	Phase D Resolved – AOT is part of product
[TBD19] Water vapor map - output	To deliver the water vapour map (forgotten)	Phase D Resolved – WV is part of product
[TBD20] List of experimental data takes	The list of imaging modes and parameters for experimental products is still to be defined	Shortly after GS CDR Resolved

Table 9-1 List of TBD

END OF DOCUMENT